

# On The Mass-to-Light Ratio of Large Scale Structure

Jeremy L. Tinker<sup>1</sup>, David H. Weinberg<sup>1</sup>, Zheng Zheng<sup>2,4</sup>, & Idit Zehavi<sup>3</sup>

## ABSTRACT

We examine the dependence of the mass-to-light ( $M/L$ ) ratio of large-scale structure on cosmological parameters, in models that are constrained to match observations of the projected galaxy correlation function  $w_p(r_p)$  and the galaxy luminosity function. For a sequence of cosmological models with a fixed, observationally motivated power spectrum shape and increasing normalization  $\sigma_8$ , we find parameters of the galaxy halo occupation distribution (HOD) that reproduce  $w_p(r_p)$  measurements as a function of luminosity from the Sloan Digital Sky Survey (SDSS). From these HOD models we calculate the  $r$ -band conditional luminosity function  $\Phi(L|M_h)$ , and from this the mean  $M/L$  ratio as a function of halo mass  $M_h$ . We also use  $\Phi(L|M_h)$  to populate halos of N-body simulations with galaxies and thereby compute  $M/L$  in a range of large-scale environments, including cluster infall regions. For all cosmological models, the  $M/L$  ratio in high mass halos or high density regions is approximately independent of halo mass or smoothing scale. However, the “plateau” value of  $M/L$  depends on  $\sigma_8$  in addition to the obvious proportionality with the matter density parameter  $\Omega_m$ , and it represents the universal value  $\langle M/L \rangle = \Omega_m \rho_{\text{crit}} / \rho_{\text{lum}}$  only for models in which the galaxy correlation function is approximately unbiased, i.e., with  $\sigma_8 \approx \sigma_{8g}$ . Our results for cluster mass halos follow the trend  $(M/L)_{\text{cl}} = 577 (\Omega_m/0.3) (\sigma_8/0.9)^{1.7} h M_\odot/L_\odot$ . Combined with Carlberg et al.’s (1996) mean  $M/L$  ratio for CNOC galaxy clusters, this relation implies  $(\sigma_8/0.9) (\Omega_m/0.3)^{0.6} = 0.75 \pm 0.06$ .  $M/L$  estimates for SDSS clusters and the virial regions of clusters in the CAIRNS survey imply a similar value of  $\sigma_8 \Omega_m^{0.6}$ , while the CAIRNS estimates for cluster infall regions imply a lower value. These results are inconsistent with parameter values  $\Omega_m \approx 0.3$ ,  $\sigma_8 \approx 0.9$  favored by recent joint analyses of cosmic microwave background measurements and other large scale structure data, though they agree with values inferred from van den Bosch et al.’s (2003) analysis of the

---

<sup>1</sup>Department of Astronomy, The Ohio State University, 140 W. 18th Avenue, Columbus, Ohio 43210

<sup>2</sup>Institute for Advanced Study, School of Natural Sciences, Einstein Drive, Princeton, NJ 08540

<sup>3</sup>Steward Observatory, University of Arizona, 933 N. Cherry Avenue, Tucson, AZ 85721

<sup>4</sup>Hubble Fellow

2dF Galaxy Redshift Survey. We discuss possible resolutions of this discrepancy, none of which seems entirely satisfactory. In appendices we present an improved formula for halo bias factors calibrated on our  $360^3$  N-body simulations and an improved analytic technique for calculating the galaxy correlation function from a given cosmological model and HOD.

*Subject headings:* cosmology: observations — cosmology: theory — galaxies: clustering — galaxies: clusters — large-scale structure of universe

## 1. Introduction

Determining the matter density of the universe is one of the key goals of observational cosmology. By definition, the mean matter density is the product of the mean luminosity density and the mean mass-to-light ratio of the universe,  $\langle M/L \rangle$ , making the density parameter

$$\Omega_m = \langle M/L \rangle \times \rho_{\text{lum}} / \rho_{\text{crit}}. \quad (1)$$

One of the classic methods of inferring  $\Omega_m$  is to estimate the  $M/L$  ratios of galaxy groups or clusters, then multiply by the mean luminosity density derived from the galaxy luminosity function (e.g., Gott et al. 1974; Peebles 1986; Bahcall et al. 1995; Carlberg et al. 1996). However, dynamical methods of estimating  $M/L$  necessarily focus on dense regions of the galaxy distribution, so this route to  $\Omega_m$  relies on the assumption that the galaxy population in these region is representative of the universe as a whole. Observed  $M/L$  ratios rise steadily from the scale of binary galaxies to groups to rich clusters, but there is an approximate plateau in  $M/L$  values for the richest bound systems, and the mass-to-light ratios inferred from the dynamics of superclusters and the extended infall regions around clusters extend this plateau to larger scales (see, e.g., Bahcall et al. 1995; Bahcall et al. 2000, hereafter B00; Rines et al. 2004). The existence of this plateau is sometimes taken as evidence that the measured values of  $M/L$  do indeed represent the universal value.

This paper has two goals. The first is to assess the above line of reasoning: does the existence of a plateau in  $M/L$  at large scales imply that the universal value has been reached? The second is to assess the implications of observed  $M/L$  ratios for the values of  $\Omega_m$  and the matter fluctuation amplitude  $\sigma_8$ , which we will show plays a crucial role. (Here  $\sigma_8$  is the rms matter fluctuation in spheres of radius  $8 h^{-1}$  Mpc, calculated from the linear matter power spectrum, where  $h \equiv H_0/100 \text{ km s}^{-1} \text{ Mpc}^{-1}$ .) The key to these assessments is a model

for the relation between galaxies and dark matter (a.k.a. galaxy bias) that extends to the non-linear regime. We will derive this relation empirically, by fitting models of the halo occupation distribution (HOD; see Berlind & Weinberg 2002 and references therein) to the projected correlation functions of galaxies in the Sloan Digital Sky Survey (SDSS; York et al. 2000), along the lines of Zehavi et al. (2004a,b). HOD models describe bias at the level of virialized halos by the probability  $P(N|M)$  that a halo of virial mass  $M$  contains  $N$  galaxies of a specified type, together with prescriptions for spatial and velocity biases within halos.

B00 also addressed the complications of mass-to-light ratios, drawing on the results of a hydrodynamic simulation of the galaxy population. Their simulation predicts a plateau in the  $B$ -band  $M/L$  that is close to the universal value, except for a modest “anti-bias” arising from the older stellar populations of galaxies in dense environments. Applying this anti-bias correction to the observed  $(M/L)_B$  values, they infer  $\Omega_m = 0.16 \pm 0.03$ . However, B00 considered only a single cosmological model, with  $\sigma_8 = 0.8$ . We will show that, when the bias relation is inferred empirically by matching the observed correlation function, a plateau in  $M/L$  at high halo masses or overdensities is a generic result. However, the plateau corresponds to the true universal  $M/L$  *only* for models with  $\sigma_8 \approx \sigma_{8g}$ , where  $\sigma_{8g}$  is the rms galaxy count fluctuation. For lower  $\sigma_8$ , galaxies must be positively biased to match the observed clustering, and the  $M/L$  plateau is below the universal value. For higher  $\sigma_8$ , the galaxy population is anti-biased in the dense regions, and the  $M/L$  plateau is higher than the universal value.

Zehavi et al. (2004b) infer HOD parameters as a function of galaxy  $r$ -band luminosity by fitting measurements of the projected galaxy correlation function  $w_p(r_p)$ , assuming a cosmological model with  $\sigma_8 = 0.9$ . We carry out a similar procedure, but we consider a range of  $\sigma_8$  values from 0.6 to 0.95. We keep the shape of the linear matter power spectrum  $P_{\text{lin}}(k)$  fixed, regardless of  $\sigma_8$  or  $\Omega_m$ , because it is well constrained empirically by the combination of microwave background anisotropies and large-scale galaxy clustering measurements (e.g., Percival et al. 2002; Spergel et al. 2003; Tegmark et al. 2004), and because the physical effects of changes in  $\Omega_m$  are much more transparent if they are kept separate from  $P_{\text{lin}}(k)$  changes<sup>1</sup>. For a specified  $\Omega_m$  and  $\sigma_8$ , we can calculate  $M/L$  as a function of halo mass analytically, given the HOD parameters derived by fitting  $w_p(r_p)$  (see §2). To compute  $M/L$  over larger scales, we use the derived HODs to populate the halos of N-body simulations.

As shown by Zheng et al. (2002), for a fixed linear power spectrum, a change to  $\Omega_m$

---

<sup>1</sup>In the inflationary cold dark matter (CDM) framework, a change in  $\Omega_m$  with all other parameters held constant alters the shape of  $P_{\text{lin}}(k)$ . However, variations other parameters, such as the Hubble constant, the inflationary spectral index, spectral running, the baryon density, and the neutrino mass can compensate for those changes, at least to some degree.

simply shifts the mass and velocity scales of virialized halos, with negligible effect on the shape of the halo mass function or the clustering of halos at a given (scaled) mass. For two cosmological models that differ only in the value of  $\Omega_m$ , we can obtain identical real-space galaxy clustering by simply shifting the HOD mass scale in proportion to  $\Omega_m$ . With bias constrained by the observed clustering, therefore, our predicted  $M/L$  ratios for a given  $\sigma_8$  are simply proportional to  $\Omega_m$ . We will often indicate this scaling by quoting predicted  $M/L$  ratios in units of  $\omega_{0.3} h M_\odot/L_\odot$ , where  $\omega_{0.3} = \Omega_m/0.3$ . The scaling with  $h$  arises in the observations because inferred dynamical masses scale as  $h^{-1}$  and luminosities as  $h^{-2}$ . The same  $h$  scaling arises in the predictions because the characteristic mass in the halo mass function is proportional to  $h^{-1}$  at fixed  $\Omega_m$  and  $\sigma_8$  and we automatically impose the observed luminosity scale, which is proportional to  $h^{-2}$ . Uncertainties in the value of  $h$  therefore have no impact on our conclusions.

Most recent applications of the mass-to-light method yield  $\Omega_m \approx 0.15 - 0.20$  (e.g., Bahcall et al. 1995; Carlberg et al. 1996; B00; Lin et al. 2003; Rines et al. 2004). Alternative methods of inferring  $\Omega_m$ , from cosmic microwave background (CMB) anisotropies, the shape of the galaxy power spectrum, Type Ia supernovae, and the baryon-to-total mass ratio in clusters, have begun to converge on a significantly higher value of  $\Omega_m \approx 0.3$  (e.g. Turner 2002). Recently Tegmark et al. (2004) combined WMAP CMB data with the SDSS galaxy power spectrum to infer  $\Omega_m = 0.30 \pm 0.04$ . Seljak et al. (2004) combined these data with the SDSS Lyman- $\alpha$  forest spectrum to obtain  $\Omega_m = 0.28 \pm 0.02$ . The tension between  $M/L$  estimates of  $\Omega_m$  and the higher values from other methods warrants a careful investigation of the assumptions that underly the  $M/L$  approach. We will show that the conflict can be alleviated if  $\sigma_8$  is low,  $\sim 0.6 - 0.7$ . However, the discrepancy persists for a matter fluctuation amplitude of  $\sigma_8 \approx 0.9$ , which is favored by the Tegmark et al. (2004) and Seljak et al. (2004) analyses.

Our approach is similar in spirit to the conditional luminosity function (CLF) analyses of clustering in the Two-Degree Field Galaxy Redshift Survey (2dFGRS; Colless et al. 2001) by Yang et al. (2003; 2004), van den Bosch et al. (2003), and Mo et al. (2004). In practice there are important differences in the two techniques. In the CLF, the luminosity function within an isolated halo is parameterized by a Schechter function, while in our approach this function is determined non-parametrically. We fit the full projected correlation function, while the above CLF papers fit the luminosity dependence of the galaxy correlation length, together with the galaxy luminosity function. Despite the many differences in analysis and parameterization, and the use of independent galaxy clustering measurements derived from an  $r$ -band selected sample instead of a  $b_J$ -selected sample, we reach a bottom line similar to that of van den Bosch et al. (2003): obtaining cluster mass-to-light ratios close to the observational estimates of  $\sim 350 h M_\odot/L_\odot$  (e.g. Carlberg et al. 1996; B00) requires either

$\Omega_m$  or  $\sigma_8$  to be significantly below the currently favored values of 0.3 and 0.9 (see §4).

## 2. HOD Modeling of $w_p(r_p)$

The key ingredient in the HOD prescription of galaxy bias is  $P(N|M)$ , the probability that a halo of mass  $M$  contains  $N$  galaxies of a specified class. The galaxy classes we will consider are defined by thresholds in  $r$ -band luminosity. Our model for  $P(N|M)$  is motivated by theoretical studies of the HOD using semi-analytic galaxy formation methods, high-resolution N-body simulations, and full hydrodynamic cosmological simulations (specifically Kravtsov et al. 2004 and Zheng et al. 2004; for earlier work see Jing et al. 1998; Kauffmann et al. 1997, 1999; Benson et al. 2000; Seljak 2000; White et al. 2001; Yoshikawa et al. 2001; Berlind et al. 2003). This model distinguishes halo central galaxies from satellites in halos containing multiple galaxies. In our standard parameterization, the number of central galaxies above the luminosity threshold changes sharply from zero to one at a minimum halo mass  $M_{\min}$ . We also consider a model in which the probability of hosting a central galaxy is  $\exp(-M_{\min}/M)$ , to test the sensitivity of our results to the assumed sharpness of the central galaxy threshold.

We adopt a functional form

$$\langle N_{\text{sat}} \rangle_M = \exp\left(-\frac{M_{\text{cut}}}{M - M_{\min}}\right) \left(\frac{M}{M_1}\right) \quad (2)$$

for the mean number of satellites in a halo of mass  $M \geq M_{\min}$ , and  $\langle N_{\text{sat}} \rangle_M = 0$  for  $M < M_{\min}$ . Here  $M_{\text{cut}}$  is a cutoff mass scale for the satellite galaxy power law, which allows a soft transition to halo masses that host no satellites. Zehavi et al. (2004b) showed that a model of this form allows good fits to the observed  $w_p(r_p)$  for the concordance cosmology, though they mainly focused on an alternative parameterization with a sharp cutoff in  $\langle N_{\text{sat}} \rangle_M$  and a free power-law index  $\langle N_{\text{sat}} \rangle_M \propto M^\alpha$ . The fixed- $\alpha$  with varying  $M_{\text{cut}}$  parameterization is better suited to our purposes here because we will difference occupation functions for adjacent luminosity thresholds to obtain  $P(N|M)$  for luminosity bins, and small statistical errors in  $\alpha$  can drastically affect the number of satellites in individual bins at high halo mass. We assume a Poisson distribution of satellite number relative to the mean  $\langle N_{\text{sat}} \rangle_M$ , as implied by the theoretical studies.

This parameterization of  $P(N|M)$ , while restricted, has the virtue of capturing theoretical predictions quite well while introducing only three free parameters. An essentially perfect fit to theoretical results requires two additional parameters providing freedom in  $\alpha$

and the central galaxy cutoff shape (Zheng et al. 2004). However, we expect the three parameter model to be adequate to our purposes here, predicting the mass-to-light ratios in and around high mass halos.

We will investigate the effects of changing the assumed value of  $\alpha$ , but we note that the choice of  $\alpha = 1$  is well motivated by the results of semi-analytic models, hydrodynamic simulations, and collisionless N-body simulations (Zheng et al. 2004; Kravtsov et al. 2004). Observational estimates of  $\alpha$  are subject to the effects of interlopers, completeness limits, and uncertainty in the halo mass estimates, and the agreement among observational estimates is not as good as for the theoretical studies. Lin et al. (2004), using a sample of rich clusters from the 2MASS survey, find  $N_{\text{sat}} \propto M^{0.87}$ , in agreement with the much smaller sample of Rines et al. (2004), who find  $\alpha = 0.84$ . Kochanek et al. (2003), who analyze a different 2MASS cluster sample, find  $\alpha = 1.1$ . Analysis of the 2dF Percolated-Inferred Galaxy Group catalog (Eke et al. 2004) by Collister & Lahav (2004), which constitutes the largest group sample analyzed to date, yields  $\alpha = 0.99$ , a value consistent with the preliminary results of the group multiplicity function for SDSS galaxies (A. Berlind, private communication).

We fit the observed  $w_p(r_p)$  for each luminosity threshold sample of SDSS galaxies measured in Zehavi et al. (2004b), as listed in their Table 2. For the  $M_r = -20$  threshold<sup>2</sup>, we use the sample limited to redshift  $z \leq 0.06$ . We fit each sample for five values of  $\sigma_8$ : 0.95, 0.9, 0.8, 0.7 and 0.6. Our results for  $\sigma_8 = 0.9$  are similar to those of Zehavi et al. (2004b), except for the slight differences in parameterization and calculational method (see Appendix B). For all calculations, we adopt a linear theory matter power spectrum with inflationary spectral index  $n_s = 1$  and shape parameter  $\Gamma = 0.2$  in the parameterization of Efstathiou et al. (1992). Satellite galaxies are assumed to follow the “universal” halo density profile of Navarro, Frenk, & White (1997) with no internal spatial bias. The halo concentrations are calculated in the same manner as Kuhlen et al. (2004) assuming  $\Omega_m = 0.3$ , with the halo edge defined as the radius at which the mean interior density is 200 times the mean value. The calculation of  $w_p(r_p)$  for a specified cosmology and HOD is described in Appendix B. Our method is similar to that of Zheng (2004), which was used by Zehavi et al. (2004b), but we implement an improved treatment of halo exclusion and adopt more accurate halo bias factors inferred from our N-body simulations (Appendix A).

The data for each luminosity threshold are fit by minimizing  $\chi^2$  using the full covariance matrix for each sample. The jackknife estimates of these matrices are discussed in detail by Zehavi et al. (2004b). The number of free parameters in the fit is reduced from three to two by matching the space density of galaxies for each sample. In practice, this constraint

---

<sup>2</sup>Throughout this paper, we quote absolute magnitudes for  $h = 1.0$ .

is used to fix the value of  $M_{\min}$  for a given  $M_{\text{cut}}$  and  $M_1$ . We ignore the uncertainty in the space density itself. We require that the number density of satellite galaxies between two adjacent magnitude limits be smaller for the brighter sample at all halo masses, a consistency condition that only affected the result in two of the 45 fits performed. The results of the fits are listed in Table 1.

Figure 1a shows two examples of these fits. The observed  $w_p(r_p)$  for  $M_r < -20$  and  $M_r < -21.5$  are shown by the symbols with error bars, plotted on top of the HOD fits for each value of  $\sigma_8$ . For  $M_r < -21.5$ , the different fits are difficult to distinguish. For  $M_r < -20$ , the larger error bars allow the best-fit HOD models to differentiate some at large scales, even though the  $\chi^2$  values per degree of freedom are all less than one. Note that strong covariances between data points make a simple visual estimate of  $\chi^2$  unreliable. In Figure 1b, the data are plotted against the nonlinear matter correlation functions for each value of  $\sigma_8$ . These correlation functions are calculated by Fourier transformation of the Smith et al. (2003) non-linear  $P(k)$ , which takes the linear power spectrum as input, and assume  $\Omega_m = 0.3$ . The differences in the matter distributions are large, but are easily overcome even with our restrictive three-parameter HOD.

The values of  $\chi^2$  per degree of freedom for the HOD fits fluctuate from sample to sample, with a median value below 1.0 for  $\sigma_8 \geq 0.8$  and above 1.0 for  $\sigma_8 \leq 0.7$ . We do not regard the somewhat higher  $\chi^2$  values as significant arguments against low  $\sigma_8$ , however, because our three-parameter description of the HOD is quite restrictive. In addition, adopting a CMBFAST (Seljak & Zaldarriaga 1996) power spectrum with the Tegmark et al. (2004) cosmological parameters in place of the  $\Gamma = 0.2$ , Efstathiou et al. (1992) power spectrum has a noticeable effect on  $\chi^2$  values, though it makes almost no difference to the best-fit HOD parameters themselves. Adding freedom to the HOD parameterization or changing the input power spectrum could thus have significant effect on the quality of the  $w_p(r_p)$  fits, but we expect only minor influence on our mass-to-light ratio predictions because the overall shape of  $\langle N \rangle_M$  is well constrained by the number density and  $w_p(r_p)$  measurements.

From the HOD fits listed in Table 1, we can calculate a discrete estimate of the conditional luminosity function,  $\Phi(L|M_h)$ , the luminosity function of galaxies in halos of mass  $M_h$ . Since the HODs describe samples brighter than a specified absolute magnitude, differencing the number of galaxies in a halo of mass  $M_h$  within the magnitude bin of width  $\Delta M_r = 0.5$  mag yields  $\Phi(L|M_h)$  within that bin:

$$\Phi(L|M_h)\Delta L = \langle N \rangle_{M_h}^{(M_r)} - \langle N \rangle_{M_h}^{(M_r - \Delta M_r)}. \quad (3)$$

We use luminosity rather than magnitude on the left hand side of equation (3) for clarity

of notation. In this form, equation (3) is normalized such that a summation of  $\Phi(L|M_h)$  over all magnitude bins returns  $\langle N \rangle_M$  for the  $M_r < -18$  sample. The parameters in Table 1 assume our standard HOD model with a sharp threshold for the central galaxy occupation. When we use an exponential cutoff for the central occupation, we keep the same values of  $M_1$  and  $M_{\text{cut}}$  but adjust  $M_{\text{min}}$  slightly so that the mean galaxy space density remains fixed.

Figure 2 plots the conditional luminosity functions for three halo masses for the exponential central cutoff. Panel (a) shows  $\Phi(L|M_h)$  for  $M_h = 3 \times 10^{12} h^{-1} M_\odot$ , normalized so that the area under each curve is the total number of galaxies expected at this halo mass. The dashed line that falls rapidly at  $M_r < -19.5$  is the satellite galaxy contribution to  $\Phi(L|M_h)$  for the model with  $\sigma_8 = 0.95$ . At this low halo mass, the number of satellite galaxies brighter than  $M_r = -18$  is smaller than the number of central galaxies, but satellites dominate at the faintest magnitudes. The variation of  $\Phi(L|M_h)$  with  $\sigma_8$  is minimal because at this point on the halo mass function the space density of halos is only weakly sensitive to  $\sigma_8$ . The difference in the total number of galaxies brighter than  $M_r = -18$  between the low and high values of  $\sigma_8$  is  $1.84 - 1.56 = 0.28$ .

Panel (b) shows  $\Phi(L|M_h)$  for  $M_h = 3 \times 10^{13} h^{-1} M_\odot$ . Halos of this mass are intermediate between those that host galaxy groups and clusters, with  $\langle N \rangle_M \approx 8$  for  $M_r \leq -18$ . Satellite galaxies dominate the conditional luminosity functions out to  $M_r = -21$ , beyond which the brighter central galaxies dominate. The different values of  $\sigma_8$  now produce small differences in the overall normalization of  $\Phi(L|M_h)$ . As  $\sigma_8$  decreases, the space density and clustering amplitude of high mass halos decreases, and the mean occupation of these halos must grow to keep the galaxy number density and clustering amplitude constant. In panel (c), which plots  $\Phi(L|M_h)$  for cluster-sized halos of  $M_h = 3 \times 10^{14} h^{-1} M_\odot$ , the differences in the models are clear. The low- $\sigma_8$  model has nearly twice as many galaxies per halo as  $\sigma_8 = 0.95$ . For all the models,  $\Phi(L|M_h)$  is dominated by satellite galaxies at all but the brightest magnitude bin.

Our eventual qualitative conclusion is already evident from Figure 2. With the galaxy space density and clustering amplitude fixed to match observations, a low- $\sigma_8$  model must have a larger fraction of its galaxies in massive halos, and it therefore predicts lower mass-to-light ratios in these halos.

To quantify this point, we calculate mass-to-light ratios as a function of halo mass by summing over luminosity,

$$M/L = M_h \left[ \sum_i L^{(i+1/2)} \left( \langle N \rangle_M^{(i)} - \langle N \rangle_M^{(i+1)} \right) \right]^{-1}, \quad (4)$$

where  $i$  denotes the magnitude threshold, which runs from  $-18$  to  $-22$ . All galaxies in each magnitude bin are assumed to be at the midpoint of the bin, and galaxies in the  $M_r < -22$  sample are assumed to have  $M_r = -22.25$ , an assumption that has negligible influence on the results. Equation (4) is equivalent to  $M/L = M_h / \int_{L_{\min}}^{L_{\max}} L \Phi(L|M_h) dL$  given our discrete estimate of  $\Phi(L|M_h)$  in equation (3).

Before proceeding to our main results, we want to check the sensitivity of our calculations to the form of the central galaxy cutoff and the value of  $\alpha$ . In Figure 3a, points with error bars are the SDSS data for  $M_r < -20$  from Zehavi et al. (2004b), and the solid line shows the fit with a hard cutoff and the parameters in Table 1 for  $\sigma_8 = 0.95$ . Filled circles show  $w_p(r_p)$  for the same values of  $M_1$  and  $M_{\text{cut}}$ , but an exponential cutoff, with  $M_{\min}$  adjusted to retain the galaxy density. The differences in the calculated correlation functions are barely discernible, mostly confined to the two-halo term at small scales, where the one-halo term dominates  $w_p(r_p)$  anyway. Figure 3b shows an example of  $\Phi(L|M_h)$  for the soft and hard central cutoffs for  $\sigma_8 = 0.95$  at  $M_h = 3 \times 10^{13} h^{-1} M_\odot$ . The low luminosity regimes are identical, but at high luminosities where central galaxies dominate, the central cutoff produces a well-defined bump, which is smoothed out in the exponential cutoff model. Panel (c) shows the mass-to-light ratio as a function of halo mass for these two prescriptions. The sharp cutoff model produces artificial jumps in the  $M/L$  function, but the overall trend and, more importantly, the behavior at high halo masses are the same for hard and soft cutoffs. We conclude that the details of the central galaxy cutoff do not significantly affect the mass-to-light ratio predictions.

In Figure 4 we quantify the dependence of our results on the value of  $\alpha$ . First, we refit  $w_p(r_p)$  and calculate  $M/L$  for  $\sigma_8 = 0.9$  with  $\alpha = 0.9, 0.95, 1.05, \text{ and } 1.1$ . The results are shown, along with the fiducial results for  $\alpha = 1$ , as the five curves in Figure 4a. The  $M/L$  ratios are nearly identical at group masses and below. At  $M \approx 2 \times 10^{14} h^{-1} M_\odot$  the curves begin to separate, with lower  $\alpha$  resulting in higher  $M/L$ , and vice versa, due to the different scalings of galaxy number with halo mass.

Our second method for testing the sensitivity to  $\alpha$  uses a much more flexible HOD parameterization in which the value of satellite mean occupation is specified at  $\log M = 12, 13, 14, \text{ and } 15$ , connected by a cubic spline and smoothly truncated at low masses (see Figure 19 of Zehavi et al. 2004b for examples of similar fits). With this extra freedom, it is difficult to guarantee that  $\langle N_{\text{sat}} \rangle_M$  is a monotonically increasing function of luminosity threshold, so we have therefore fit the Zehavi et al. (2004b) measurements for samples in absolute magnitude bins, rather than magnitude thresholds. In each bin, we assume that  $\langle N_{\text{cen}} \rangle_M = 1$  in a range  $M_{c,\min} - M_{c,\max}$  and  $\langle N_{\text{cen}} \rangle_M = 0$  elsewhere, equivalent to our sharp cutoff assumption for luminosity threshold samples. Using a Monte Carlo Markov Chain

(e.g., Lewis & Bridle 2002), we identify between 17 and 42 models for each luminosity bin that have  $\Delta\chi^2 \leq 1$  relative to the best fit model. Using all  $4.7 \times 10^6$  possible combinations of these models, we evaluate the  $M/L$  ratios at the cluster mass scale. The distribution of  $M/L$  values with respect to the mean at a given mass has an approximately Gaussian core with a half-width of 11% at 10% of the maximum. At lower probabilities, there is a tail toward high  $M/L$  values that arises from HOD fits that are statistically acceptable but physically implausible, with anomalously high halo masses for central galaxies. There is no corresponding tail to low  $M/L$  values, since if one puts too many galaxies in clusters the correlation function is inevitably too high. The shaded region in Figure 4a shows the full-width at 10% maximum as a function of halo mass. This test also accounts for statistical uncertainty in the  $w_p(r_p)$  measurements themselves.

Figure 4b quantifies the change in the average cluster  $M/L$  as a function of  $\alpha$ . The  $y$ -axis shows the percentage difference in  $(M/L)_{\text{cl}}$ , averaged over the halo masses of the CNOC cluster sample (see §3.2 below), with respect to  $\alpha = 1.0$ . For  $\Delta\alpha = 0.1$ ,  $\Delta(M/L)_{\text{cl}} \approx 8\%$ , and for  $\Delta\alpha = 0.05$ ,  $\Delta(M/L)_{\text{cl}} \approx 4\%$ . Although the differences in the  $M/L$  curves of panel (a) appear large at the highest halo mass, the impact of these differences is moderated in panel (b) because clusters above  $10^{15} h^{-1} M_\odot$  are relatively rare. We conclude that for any given cosmology, the existing  $w_p(r_p)$  measurements constrain the average cluster mass-to-light ratio, the quantity most relevant to our conclusions, to within about 10%. However, the detailed shape of the  $M/L$  curve at  $M_h > 3 \times 10^{13} h^{-1} M_\odot$  depends on the assumed form of the HOD.

### 3. Mass-to-Light Ratios of Large-Scale Structure

#### 3.1. $M/L$ vs. overdensity

The numerical results in this and subsequent sections are calculated using Tinker, Weinberg, & Zheng’s (2004)  $\Lambda$ CDM simulations (inflationary cold dark matter with a cosmological constant). These simulations, consisting of a set of 5 realizations of  $360^3$  particles evolved in a periodic volume  $253 h^{-1} \text{Mpc}$  on a side, have the appropriate mass resolution for modeling the luminosity-dependent  $\xi_g(r)$  of galaxies with  $M_r \leq -20$ . Fainter samples have minimum halo masses below the smallest resolved halos in our simulations, which are identified using a friends-of-friends algorithm with a minimum of 30 particles. The dark matter power spectrum used to create the initial conditions is identical to that assumed in the analytic HOD calculations of the previous section. These simulations are run with GADGET (Springel, Yoshida, & White 2000), with a force softening of  $70 h^{-1} \text{kpc}$ , and the standard GADGET timestep criterion  $\eta = 0.2$ . The simulations have  $\Omega_m = 0.1$ ,  $\Lambda = 0.9$ , and  $\sigma_8 = 0.95$  at the

Table 1. HOD Parameters for the SDSS Galaxy Samples

$M_r$	$M_{\min}$	$M_{\text{cut}}$	$M_1$	$\chi^2_{dof}$	$M_{\min}$	$M_{\text{cut}}$	$M_1$	$\chi^2_{dof}$	$M_{\min}$	$M_{\text{cut}}$	$M_1$	$\chi^2_{dof}$	
				$\sigma_8=0.95$					$\sigma_8=0.9$				
-18.0	11.2	12.0	12.7	1.63	11.3	11.7	12.7	1.40	11.3	12.1	12.6	1.11	
-18.5	11.4	12.3	12.8	0.88	11.4	12.3	12.7	0.72	11.4	12.7	12.6	0.49	
-19.0	11.5	12.7	12.8	0.94	11.5	12.7	12.8	0.90	11.5	12.9	12.7	1.04	
-19.5	11.7	13.1	13.0	0.22	11.7	13.1	12.9	0.22	11.7	13.1	12.9	0.51	
-20.0	12.0	13.0	13.3	0.51	12.0	13.0	13.2	0.51	12.0	13.2	13.1	0.58	
-20.5	12.3	13.1	13.5	1.80	12.3	13.2	13.4	2.21	12.3	13.3	13.4	3.09	
-21.0	12.7	13.6	13.9	1.28	12.7	13.6	13.8	1.36	12.7	13.7	13.7	1.58	
-21.5	13.3	14.6	14.1	0.94	13.3	14.6	14.0	0.90	13.2	14.6	13.8	0.86	
-22.0	13.9	14.8	14.6	1.42	13.9	14.7	14.5	1.42	13.8	14.9	14.2	1.27	
				$\sigma_8=0.7$					$\sigma_8=0.6$				
-18.0	11.3	12.1	12.5	0.96	11.3	12.1	12.4	0.94					
-18.5	11.4	12.6	12.6	0.43	11.4	12.5	12.5	0.61					
-19.0	11.5	12.8	12.7	1.43	11.5	12.7	12.6	2.11					
-19.5	11.7	13.0	12.8	1.17	11.7	12.9	12.7	1.98					
-20.0	12.0	13.1	13.0	0.70	12.0	13.2	12.9	0.91					
-20.5	12.3	13.3	13.3	3.97	12.2	13.3	13.1	5.02					
-21.0	12.7	13.6	13.6	1.86	12.6	13.7	13.4	2.31					
-21.5	13.2	14.5	13.6	0.88	13.1	14.5	13.4	1.00					
-22.0	13.7	14.9	13.8	0.97	13.6	14.6	13.8	0.74					

Note. — Values of  $M_{\min}$ ,  $M_{\text{cut}}$ , and  $M_1$  are listed as  $\log(M/h^{-1}M_{\odot})$

last output, and we use earlier outputs to represent  $z = 0$  results for lower  $\sigma_8$ , rescaling halo masses as necessary to represent different  $\Omega_m$  (see Zheng et al. 2002 and Tinker et al. 2005 for further discussion). For the purposes of this paper, this rescaling approach should yield nearly identical results to running separate simulations for each  $(\Omega_m, \sigma_8)$  combination, since at fixed  $\sigma_8$  and  $P_{\text{lin}}(k)$  the value of  $\Omega_m$  slightly alters the density profiles of halos but has minimal impact of the halo masses and clustering.

Since  $\Phi(L|M_h)$  is known from the fits to  $w_p(r_p)$ , it is a simple process to create galaxy distributions from the dark matter halo populations in the simulations. These galaxy distributions will match both the SDSS clustering and luminosity function for all values of  $\sigma_8$ . For each halo above  $M_{\text{min}}$  (for the  $M_r < -20$  sample), the central galaxy is placed at the center of the halo, which we define as the location of the most-bound dark matter particle, i.e., the particle with the most negative potential energy calculated by a Newtonian summation over all the particles in the halo. The number of satellite galaxies is chosen from a Poisson distribution with a mean given by equation (2), and the satellites are spatially distributed by random sampling of the dark matter particles in the halo (other than the most-bound particle). The luminosities of the galaxies are selected at random from  $\Phi(L|M_h)$ , truncated at  $M_r = -20$ . Since central and satellite galaxies have distinct contributions to  $\Phi(L|M_h)$ , in practice they are treated separately when populating the N-body halos; central galaxy luminosities are chosen only from their contribution to the total  $\Phi(L|M_h)$ , while satellite luminosities are chosen from the satellite galaxy portion of  $\Phi(L|M_h)$ .

The halo mass function in the simulations differs from the analytic form of Jenkins et al. (2001) at some masses. The discrepancy is within the range shown in Jenkins et al.’s Figure 8, but at the high end, with maximum difference of 10-15% in number of halos at fixed mass. Using our analytically derived HOD parameters, which assume the Jenkins et al. (2001) form, therefore leads to  $\sim 7.5\%$  too many galaxies (relative to the observed space density we are trying to match) when we populate the simulations. We correct for this discrepancy when populating the N-body simulations by changing  $M_{\text{min}}$  for each sample to the value that yields the correct number of galaxies. This change is moderate,  $\lesssim 10\%$  in  $M_{\text{min}}$ , but it is required in order for the luminosity function in the simulations to accurately represent that of the Zehavi et al. (2004b) samples.

A simple application of these galaxy distributions is to investigate mass-to-light ratios as a function of overdensity in randomly placed spheres, as done by B00 using their hydrodynamic simulation. Figure 5 plots the mass-to-light ratio, relative to the mean  $M/L$  of the box, as a function of dark matter density at three top-hat smoothing scales. (In this way of plotting our data, values greater than one would be considered “anti-biased” by the definition of B00, since luminosity enters in the denominator). For each  $\delta$ , the average light and

mass are calculated separately and then used to calculate  $M/L$ . This prevents divergence in spheres with no galaxies, but in practice it does not noticeably change the curves. Panel (a) shows the results for a top-hat smoothing scale of  $1.5 h^{-1} \text{Mpc}$ , the scale used by Abell (1958) to define galaxy clusters, which is close to the virial radius of  $\sim 10^{15} h^{-1} M_{\odot}$  halos. The curves shoot up at  $\delta \lesssim 0$ , since at these overdensities there are no halos above  $M_{\text{min}}$  and therefore no galaxies, so  $\rho_{\text{lum}}$  approaches zero faster than  $\rho_m$ . The exact value of  $\delta$  at which this upturn occurs depends on the adopted luminosity threshold, since fainter galaxies occupy lower mass halos, and on the smoothing radius, since the probability of finding no halos above  $M_{\text{min}}$  drops with increasing radius. The sharpness of the upturn depends on the sharpness of the  $\langle N \rangle_M$  threshold at  $M_{\text{min}}$ , but the qualitative behavior at  $\delta \lesssim 0$  is a generic prediction of any model with a minimum halo mass. In the range  $0 \lesssim \delta \lesssim 10$ , all the curves dip below the mean due to low-mass halos that host a central galaxy. Overdensities of  $\delta \gtrsim 100$  begin to represent virialized, cluster-like structures. At this  $\delta$ , the different  $\sigma_8$  models spread out, with high- $\sigma_8$  having  $M/L$  ratios above or equal to the mean and low- $\sigma_8$  models having  $M/L$  as low as half the global mean. Panels (b) and (c) show the same results but for smoothing scales of 5 and 10  $h^{-1} \text{Mpc}$ . For both of these smoothing scales, the different  $\sigma_8$  models diverge at the highest overdensities, with low  $\sigma_8$  corresponding to  $M/L$  ratios below the mean of simulation. At the highest overdensities, most of the  $M/L$  curves flatten to a roughly constant value, though for low  $\sigma_8$  and large smoothing scale the  $M/L$  ratio is a declining function of  $\delta$  in this regime. More importantly, the values of  $M/L$  at high  $\delta$  are nearly independent of the smoothing scale for a given model, even when they are far from the universal value.

The implications of Figure 5 are clear. The existence of a plateau in  $M/L$ , either as a function of  $\delta$  at fixed smoothing length or as a function of smoothing scale at fixed  $\delta$ , cannot be taken as evidence that one has measured the universal value of  $M/L$ . Simply measuring  $M/L$  in a large volume does not guarantee convergence to the universal  $\langle M/L \rangle$  if the measurements are made only in dense regions, where galaxies may be over- or under-represented, depending on the cosmological model. Given the level of galaxy clustering in the SDSS, the plateau in  $M/L$ , for galaxies brighter than  $M_r = -20$ , should be similar to the universal mean if  $\sigma_8 = 0.9$ , above the universal mean if  $\sigma_8 > 0.9$ , and below the universal mean if  $\sigma_8 < 0.9$ . As we will demonstrate in the next section, the value of  $\sigma_8$  for which the plateau is equal to the universal value depends on the bias of the galaxy sample under consideration, so for fainter luminosity thresholds the “unbiased” value of  $\sigma_8$  is lower.

### 3.2. $M/L$ of Clusters

The  $M/L$  ratios shown in Figure 5, averaged over top-hat spheres of constant  $\delta$ , are not directly observable. In Figure 6, we make quantitative predictions for cluster sized halos that can be compared to observational data. For each  $\sigma_8$ , equation (4) is used to calculate  $M/L$  as a function of halo mass. Note that this calculation does not use simulations, so it can include galaxies down to  $M_r = -18$ . We present predictions for galaxies with  $M_r < -18$  and for galaxies with  $M_r < -20$ , and refer to these mass-to-light ratios as  $M/L_{18}$  and  $M/L_{20}$ , respectively.

Figure 6a plots  $M/L_{18}$ , calculated using the soft central cutoff, against halo mass for all values of  $\sigma_8$ . Note that halo masses are proportional to  $\Omega_m$  for fixed  $\sigma_8$ , so we list masses in  $\omega_{0.3} h^{-1} M_\odot$  and mass-to-light ratios in  $\omega_{0.3} h M_\odot/L_\odot$ . The  $M/L$  vs.  $M_h$  curves derived from our modeling of  $w_p(r_p)$  are similar in form to the parameterized function used by Yang et al. (2002) in their CLF modeling, and to the results of semi-analytic modeling by Benson et al. (2000). All the curves in panel (a) show a clear minimum at  $\sim 4 \times 10^{11} \omega_{0.3} h^{-1} M_\odot$ . Below this minimum halo mass,  $M/L_{18}$  increases rapidly, as it must to match the observed galaxy luminosity function to the steeper, low mass end of the halo mass function (see, e.g., Yang et al. 2002). At higher halo masses,  $M/L$  rises less rapidly and eventually reaches a maximum between  $1 - 5 \times 10^{14} \omega_{0.3} h^{-1} M_\odot$ , with higher values of  $\sigma_8$  reaching maximum  $M/L_{18}$  at higher masses. At still higher masses,  $M/L_{18}$  gradually declines, with the results for  $\sigma_8 = 0.6$  falling by  $\sim 20\%$  between  $10^{14} h^{-1} M_\odot$  and  $10^{15} h^{-1} M_\odot$ .

The mean mass-to-light ratio of the universe, for galaxies brighter than  $M_r < -18$ , can be calculated by integrating the Blanton et al. (2003) Schechter function fit to the observed  $r$ -band luminosity function of SDSS galaxies. This gives a luminosity density of  $1.63 \times 10^8 h L_\odot \text{Mpc}^{-3}$ , using an  $r$ -band absolute magnitude of the sun of 4.76, also taken from Blanton et al. (2003). Dividing the matter density,  $\rho_m = \Omega_m \times \rho_{\text{crit}} = 2.78 \times 10^{11} h^2 \Omega_m M_\odot \text{Mpc}^{-3}$ , by this luminosity density gives the mean  $r$ -band mass-to-light ratio of the universe,  $509 \omega_{0.3} h M_\odot/L_\odot$ .<sup>3</sup> A similar value of  $521 \omega_{0.3} h M_\odot/L_\odot$  is obtained by simply taking the number density in each magnitude bin listed in Zehavi et al. (2004b) Table 2 and using a discrete sum over all nine bins. The results in Figure 6a are similar to those of Figure 5a, but with a different model being unbiased with respect to  $\langle M/L \rangle$ ; the halos above  $10^{14} h^{-1} M_\odot$  for the  $\sigma_8 = 0.8$  model have  $M/L_{18} \approx 490 \omega_{0.3} h M_\odot/L_\odot$ , which is very close to the cosmic mean value. For  $\sigma_8$  above and below 0.8, the cluster  $M/L_{18}$  ratios are above and below this mean.

---

<sup>3</sup>To be precise, note that the Blanton et al. (2003) luminosity function is calculated in  $^{0.1}r$ , the SDSS  $r$ -band redshifted to  $z = 0.1$ , and that this shifted bandpass is also used to define the luminosity threshold samples in Zehavi et al. (2004b).

Also plotted in Figure 6a are data from the Carlberg et al. (1996) analysis of clusters from the CNOC survey, with  $M/L$  in Gunn  $r$ -band calculated using mass estimates from the virial theorem. To properly compare our calculations to their results we have taken the values listed in their Table 4, which have been extrapolated to include all luminosities below their magnitude limit of  $-18.5$  (a  $\sim 15\%$  correction), and removed most of this correction up to our magnitude limit of  $-18.0$  using the Schechter function parameters listed in their paper. This correction increases  $M/L$  ratios by  $6\%$  relative to their stated values. We have also included a moderate correction for redshift evolution, since the mean redshift of the CNOC data is  $z = 0.3$ , while the SDSS data are centered on  $z = 0.1$ . Using the approximate correction factor of  $10^{0.15\Delta z}$  (Carlberg et al. 1996) we applied an additional  $7\%$  reduction of the luminosities. We ignore the slight differences between Gunn  $r$  and SDSS  $^{0.1}r$ , which should be largely removed by the correction to solar units. The error-weighted mean of the Carlberg et al. data is  $359 \pm 32 h M_{\odot}/L_{\odot}$ .<sup>4</sup> Inserting this value into equation (1), i.e., assuming that it represents  $\langle M/L \rangle$ , gives  $\Omega_m \approx 0.2$ . However, Figure 6a demonstrates that the CNOC results are consistent with  $\Omega_m = 0.3$  if  $\sigma_8 \approx 0.65$ , since the cluster  $M/L$  is then below the universal value.

A number of authors have reported a trend of increasing  $M/L$  with cluster mass (e.g., Bahcall & Comerford 2002; Lin et al. 2004; Popesso et al. 2004), a result seemingly in conflict with the claimed plateau of  $M/L$  at high mass and with our results here. In the observational data and in our  $M/L$  curves, there is a significant increase in  $M/L$  from group masses ( $\sim 10^{13} h^{-1} M_{\odot}$ ) to the cluster mass regime. At  $M \gtrsim 10^{14} h^{-1} M_{\odot}$ , the observational data of Bahcall & Comerford (2002) and Popesso et al. (2004) are consistent with a horizontal line. Lin et al. (2004) find a positive slope well into the cluster mass regime, but Kochanek et al. (2003), analyzing a similar sample with different methods, find a *decrease* in  $M/L$  with cluster mass, suggesting a significant systematic uncertainty in the detailed behavior at high masses. Our predicted  $M/L$  curves imply that a single relation between  $M$  and  $M/L$  is a poor approximation for any samples that extend below  $\sim 2 \times 10^{14} h^{-1} M_{\odot}$ . Because of the observational uncertainties in the  $M/L$  trend and the dependence of the predicted trend on the assumed value of  $\alpha$  (see Figure 4a), we do not use this trend to draw cosmological conclusions. Instead, we use only the mean  $M/L$  in the cluster mass regime, a quantity that is more robust observationally and theoretically (see Figure 4b).

Panel (b) of Figure 6 shows the same calculation as panel (a), but now we only consider galaxies brighter than  $M_r = -20$ . Using the Blanton et al. (2003) luminosity function, the mean  $M/L$  of the universe for this magnitude threshold is  $923 \omega_{0.3} h M_{\odot}/L_{\odot}$ . The predicted

---

<sup>4</sup>This mean value does not include the two clusters from the sample that show strong binarity. The error is computed by the bootstrap method.

$M/L$  ratios still separate at high mass in the same proportions as in panel (a), but now the  $\sigma_8$  for which  $(M/L)_{cl} \approx \langle M/L \rangle$  is 0.9 instead of 0.8 for  $M/L_{18}$ , as with the numerical results presented in Figure 5.

Figure 6c plots  $M/L_{18}$  against galaxy multiplicity rather than halo mass. We compute this relation by integrating over the halo mass function to calculate the contribution of each halo mass to the abundance of clusters at a given  $N_{gal}$ , i.e.

$$M/L_{18}(N_{gal}) = \frac{\int P(N_{gal}|M) (M/L)_M \frac{dn}{dM} dM}{\int P(N_{gal}|M) \frac{dn}{dM} dM}, \quad (5)$$

where all values with a subscript  $M$  are values at a given halo mass and  $dn/dM$  is the Jenkins et al. (2001) halo mass function. The probability  $P(N_{gal}|M) = \langle N_{sat} \rangle_M^{N_{gal}-1} e^{-\langle N_{sat} \rangle_M} / (N_{gal} - 1)!$  for  $M \geq M_{min}$ , since the distribution of satellite numbers is Poisson, and a halo with a satellite has a central galaxy by definition. Because of the exponential cutoff at the high-mass end of the halo mass function, there is asymmetric scatter into a given value of  $N_{gal}$ ; Poisson fluctuations around  $\langle N \rangle_M$  cause more halos of lower mass to scatter to high  $N_{gal}$  than vice versa. This effect flattens out the curves relative to those of panel (a), but the asymptotic behavior at high multiplicity is similar.

Figure 6d shows the same calculation for  $M/L_{20}$  rather than  $M/L_{18}$ . At the same halo mass, the number of galaxies with  $M_r < -18$  is roughly five times the number with  $M_r < -20$ , which is why the  $M/L$  curves reach their asymptotic values at  $N_{gal} \sim 20$  rather than  $\sim 100$ . As in panel (b), the asymptotic value of  $M/L$  for  $\sigma_8 = 0.9$  is closest to the mean value.

Figure 6d can be compared to the results from Bahcall et al. (2003a) analysis of clusters in the SDSS Early Data Release. We consider the cluster sample identified by the maxBCG method (see, e.g. Hansen et al. 2004), which characterizes richness by  $N_{BCG}$ , the number of galaxies close to the brightest galaxy in a restricted region of color-magnitude space. Bahcall et al. (2003a) report scaling relations

$$L_{0.6}^r (10^{10} L_{\odot}) = 1.42 N_{BCG}, \quad (6)$$

$$\sigma_v (\text{km s}^{-1}) = 93 N_{BCG}^{0.56}, \quad (7)$$

for luminosity and velocity dispersion as a function of  $N_{BCG}$ . We have used the Schechter function parameters given in Bahcall et al. (2003a) to correct equation (6) from their observed

limit of  $M_r = -19.8$  to our threshold of  $M_r = -20$ . The subscript 0.6 indicates that the luminosity is the total value within  $0.6 h^{-1}$  Mpc of the cluster center, the radius at which all the cluster attributes are calculated by Bahcall et al. (2003a). The velocity dispersion can be converted to mass through a relation calibrated on gravitational lensing measurements of cluster masses (Bahcall et al. 2003b):

$$M_h(r < 0.6 h^{-1}\text{Mpc}) = 3.28 \times 10^9 \sigma_v^{1.67} k_\delta h^{-1} M_\odot, \quad (8)$$

where  $k_\delta$  is a small correction factor that depends on the mean overdensity of the halo within the defined radius (see Evrard, Metzler, & Navarro 1996). Since  $k_\delta$  requires knowledge of the halo mass, we solve equation (8) by iteration, then combine with equation (6) to obtain  $M/L_{20}$  for  $8 \leq N_{\text{BCG}} \leq 40$ , the range over which the scaling functions are valid. We convert from  $N_{\text{BCG}}$  to the number of galaxies above  $M_r = -20$  using  $N_{\text{gal}} = 0.14 N_{\text{BCG}}^{1.8}$ , an approximate scaling determined from the dependence of the mean cluster luminosity function on  $N_{\text{BCG}}$  (Wechsler et al. 2004).

The shaded region in Figure 6d encloses the mean relation derived from equations (6)–(8) and is bounded by the 2-sigma errors on the scaling coefficient in equation (6). To make this comparison, we have also assumed that  $M/L_{20}$  does not vary from  $0.6 h^{-1}$  Mpc to the edge of the cluster. In our simulations, we find a modest increase in  $M/L$  from  $0.6$  to  $1.5 h^{-1}$  Mpc of about 20%, due to the bright central galaxy in each halo. The large contribution of the central galaxy to the overall luminosity of the cluster is also seen in the cluster luminosity functions of Hansen et al. (2004). However, the trend with radius is much smaller than the statistical errors on the scaling relations themselves.

There are significant systematic uncertainties in our comparison because we combine scaling relations that have large individual uncertainties and intrinsic scatter. Future  $M/L$  measurements for larger SDSS cluster samples will enable more direct comparisons. For the current data, the mean relation plotted in Figure 6b seems consistent with the Carlberg et al. (1996) results. For a universe with  $\Omega_m = 0.3$ , the mean relation is consistent with  $\sigma_8 = 0.6$ , while a lower value of  $\Omega_m \approx 0.12$  is required to match the observations for  $\sigma_8 = 0.9$ .

At high halo masses, the values of  $M/L_{18}$  and  $M/L_{20}$  are close to the universal values for  $\sigma_8 = 0.8$  and  $\sigma_8 = 0.9$ , respectively. The difference reflects the higher amplitude correlation function of more luminous galaxies. For a given value of  $\sigma_8$ , reproducing this trend requires putting a larger fraction of the more luminous galaxies in the strongly clustered, high mass halos. On large scales, the galaxy correlation function is  $\xi_{gg} = b_g^2 \xi_{mm}$ , where the galaxy bias factor  $b_g$  is a number-weighted average of the halo bias factor  $b_h(M)$ :

$$b_g = \bar{n}_g^{-1} \int_{M_{\min}}^{\infty} b_h(M) \langle N \rangle_M \frac{dn}{dM} dM, \quad (9)$$

where  $\bar{n}_g$  is the mean galaxy number density. Figure 7 plots  $b_g$  for luminosity thresholds  $M_r = -18, -19, \text{ and } -20$ , against the ratio  $(M/L)_{\text{cl}} \div \langle M/L \rangle$ , where  $(M/L)_{\text{cl}}$  is evaluated at  $M = 5 \times 10^{14} \omega_{0.3} h^{-1} M_{\odot}$  and  $\langle M/L \rangle$  is the universal mass-to-light ratio. For a given luminosity threshold,  $b_g$  and  $(M/L)_{\text{cl}}$  are decreasing and increasing functions of  $\sigma_8$ , respectively, since matching the observed galaxy correlation function requires a lower bias factor for higher  $\sigma_8$ , and a lower bias factor implies a smaller fraction of galaxies in high mass halos. At fixed  $\sigma_8$ ,  $b_g$  must be larger for high luminosity thresholds, and  $(M/L)_{\text{cl}} \div \langle M/L \rangle$  is correspondingly lower. In practice, we find in Figure 7 that  $(M/L)_{\text{cl}} \approx \langle M/L \rangle$  for the value of  $\sigma_8$  that has  $b_g \approx 1$ . There is no reason this must be exactly true, but our results are well captured by a simple rule of thumb: the cluster mass-to-light ratios for a given luminosity threshold and  $\sigma_8$  are below the universal value if the large scale galaxy correlation function is positively biased, above the universal value if the correlation function is anti-biased, and equal to the universal value if the correlation function is unbiased.

### 3.3. $M/L$ in cluster infall regions

Attempts to measure  $M/L$  of cosmic structure often focus on galaxy clusters, since their masses can be estimated by the virial theorem, by more general dynamical models (e.g., Carlberg et al. 1997), by modeling their X-ray emission, or by weak gravitational lensing. Outside the virial region, there is still matter that is gravitationally bound to the cluster, but it is not in dynamical equilibrium, so the above methods (with the exception of weak lensing) are inapplicable. At the boundary of the infall region, where peculiar velocity cancels Hubble flow, the galaxy phase space density becomes infinite, creating caustic-like features in redshift space. The amplitude of these caustics is a measure of the escape velocity of the system (Kaiser 1987; Diaferio & Geller 1997; Diaferio 1999). The goal of the CAIRNS survey (Rines et al. 2003, 2004) was to identify these features and thereby measure the mass profile of clusters out to  $r \sim 10 h^{-1} \text{ Mpc}$ .

To compare our predictions to the results of the CAIRNS survey, we identify cluster-mass halos ( $M \geq 3 \times 10^{14} h^{-1} M_{\odot}$ ) in our N-body simulations and calculate the average  $M/L$  ratio as a function of radius. Since the CAIRNS sample is taken from 2MASS  $K$ -band data, the  $M/L$  ratios need to be converted to  $r$ -band. The total luminosities listed in Table 8 of Rines et al. (2004) are in solar  $K$ -band units, corrected for incompleteness. Using  $r - K$  colors of 1.43 for the sun and 2.81 for elliptical galaxies (Pahre 1999), we multiply

$(M/L)_K$  by  $10^{0.4(2.81-1.43)} = 3.57$  to get  $(M/L)_r$ . We have multiplied each  $M/L$  ratio by 1.7 to remove the luminosity from galaxies fainter than  $M_K = -22.81$  for a proper comparison to our  $M_r < -20$  predictions.

The CAIRNS  $M/L$  ratios have a specific geometry: the total light is in cylinders and the mass is in spheres. We calculate  $M/L_{20}$  ratios from our N-body simulations in the same way: centering on the most-bound particle of each halo with mass larger than  $3 \times 10^{14} h^{-1} M_\odot$ , the light at each projected radius  $r_p$  is calculated within a cylinder that is extended  $10 h^{-1} \text{Mpc}$  in either direction from the cluster center, using the  $z$ -axis of the box as the line of sight. The total mass in dark matter particles is calculated in spheres of radius  $r_p$ . The results for all  $\sigma_8$  values are shown in Figure 8. The ratio of these different geometries lowers  $M/L_{20}$ , since the volume of the cylinder is larger than that of the sphere. In this spheres-on-cylinders calculation, the  $M/L_{20}$  values at  $3 < r_p < 10 h^{-1} \text{Mpc}$  are lower than the mean, in contrast to the previous results. In tests that use equal cylinders for both light and mass, the  $M/L_{20}$  values, relative to the mean of the box, appear much as they did in Figure 6, with the  $\sigma_8 = 0.9$  model lying closest to the universal  $M/L$  at large  $r_p$ .

Points with error bars represent the CAIRNS measurements at  $r_{200}$  (stars) and cluster turnaround radii (squares), taken from Table 8 of Rines et al. (2004) and converted to  $r$ -band as described above. Here  $r_{200}$  is the radius at which the overdensity of the cluster is 200 times the *critical* density (666 times the mean density assuming  $\Omega_m = 0.3$ ), which is close to  $1 h^{-1} \text{Mpc}$  for all the clusters in the CAIRNS sample. The error-weighted mean of the  $r_{200}$  results is  $424 \pm 37 h M_\odot/L_\odot$ . For  $\Omega_m = 0.3$ , this value for  $(M/L_{20})_{\text{cl}}$  implies  $\sigma_8 \approx 0.7$ , similar to the CNOC results and the SDSS results shown in Figure 6. For  $\sigma_8 \approx 0.9$ , a value of  $\Omega_m \approx 0.18$  is required to bring the numerical results into agreement with the data. The error-weighted mean of the  $M/L_{20}$  values from the cluster+infall regions is significantly lower,  $313 \pm 32 h M_\odot/L_\odot$ . For  $\sigma_8 = 0.9$ , this ratio implies  $\Omega_m \approx 0.14$ .

The discrepant conclusions between the virial and infall mass estimates suggest that the mass profiles inferred by Rines et al. (2004) are steeper than those predicted by our simulations. To investigate this point further, we plot in Figure 9 the ratio of the mass  $M_{\text{tot}}$  within the turnaround radius  $r_{\text{max}}$  to the mass  $M_{200}$  within  $r_{200}$ , as a function of  $r_{\text{max}}$ . The observationally inferred mass ratios lie in the range 1.2 to 2.2, with a trend of larger mass ratios for increasing  $r_{\text{max}}$ . Solid curves show the results for our simulated clusters. While  $M_{\text{tot}}$  and  $M_{200}$  in our simulations both scale with  $\Omega_m$ , there is still a small dependence on  $\Omega_m$  because we choose clusters above  $3 \times 10^{14} h^{-1} M_\odot$ , and therefore select a different sample for different  $\Omega_m$ . Note that the observational data points are independent of the galaxy luminosity measurements and the theoretical curves are independent of our galaxy bias models, since there ratios refer to mass alone. The theoretical curves lie above the data

points by  $\sim 50\%$ , similar to the difference between the average virial and infall mass-to-light ratios. Our best guess is that the caustic method systematically underestimates the infall masses by  $\sim 50\%$ , but it is of course possible that the observationally inferred mass profiles are correct and conflict with the generic predictions of the  $\Lambda$ CDM model.

#### 4. Implications and Outlook

We have examined mass-to-light ratios of large scale structure in cosmological models that are constrained to match observed real space galaxy clustering. Specifically, we consider models in which the shape of the linear matter power spectrum is held fixed and the galaxy halo occupation distribution is adjusted to reproduce Zehavi et al.’s (2004b) measurements of the projected galaxy correlation function. For power spectrum normalization  $\sigma_8$  in the range  $0.6 - 0.95$ , we are able to find HOD parameters that yield acceptable fits to the observed  $w_p(r_p)$ , even with a restricted, 3-parameter HOD prescription. For each value of  $\sigma_8$ , the  $M/L$  ratios in high overdensity regions are approximately independent of top-hat smoothing scale in the range  $1.5 - 10h^{-1}$  Mpc, and the  $M/L$  ratios of virialized halos climb from a minimum at  $M_h \sim \text{several} \times 10^{11} h M_\odot/L_\odot$  to an approximately flat plateau in the cluster mass regime. However, this plateau only corresponds to the true universal  $M/L$  for a particular choice of  $\sigma_8$ , the one for which the large scale galaxy correlation function is unbiased. One therefore cannot take the existence of a plateau in  $M/L$  as a function of scale or of halo mass as evidence that one has measured the universal  $M/L$ . Estimates of  $\Omega_m$  that multiply cluster mass-to-light ratios by the observed luminosity density make the implicit assumption that the galaxy distribution is unbiased.

Given the SDSS clustering measurements, we expect cluster mass-to-light ratios to be representative of the universal value for  $\sigma_8 \approx 0.8$  if one is considering galaxies with  $M_r \leq -18$ , or for  $\sigma_8 \approx 0.9$  if one is considering galaxies with  $M_r \leq -20$ . For lower  $\sigma_8$ , cluster  $M/L$  ratios lie below the universal value because galaxies must be overrepresented in dense regions to match the observed clustering. Conversely, cluster  $M/L$  ratios lie above the universal value for higher  $\sigma_8$ .

Averaging our results over the same masses as the CNOC cluster sample, our results are well described by the relations

$$(M/L_{18})_{\text{cl}} = 577 \left(\frac{\sigma_8}{0.9}\right)^{1.7} \left(\frac{\Omega_m}{0.3}\right) h M_\odot/L_\odot, \quad (10)$$

$$(M/L_{20})_{\text{cl}} = 907 \left(\frac{\sigma_8}{0.9}\right)^{2.1} \left(\frac{\Omega_m}{0.3}\right) h M_\odot/L_\odot, \quad (11)$$

for luminosity thresholds of  $M_r = -18$  and  $M_r = -20$ , respectively. As discussed in §2, we estimate that uncertainties in the HOD fits introduce a  $\sim 10\%$  systematic uncertainty in the normalization of these relations, though our present investigation is not exhaustive. The luminosity function of SDSS galaxies implies universal mass-to-light ratios of  $\langle M/L_{18} \rangle = 509\omega_{0.3} h M_\odot/L_\odot$  and  $\langle M/L_{20} \rangle = 923\omega_{0.3} h M_\odot/L_\odot$ , where  $\omega_{0.3} \equiv \Omega_m/0.3$ . The statistical uncertainty in Blanton et al.’s (2003) luminosity density estimate implies a 2% uncertainty in  $\langle M/L \rangle$ .

If we combine equation (10) with the mean mass-to-light ratio of CNOC clusters,  $(M/L_{18})_{\text{cl}} = 359 \pm 32 h M_\odot/L_\odot$ , we obtain the constraint

$$\left(\frac{\sigma_8}{0.9}\right) \left(\frac{\Omega_m}{0.3}\right)^{0.6} = 0.75 \pm 0.06, \quad (12)$$

or  $\sigma_8 \Omega_m^{0.6} = 0.33 \pm 0.03$ . Here we have added in quadrature the 9% statistical error on the mean cluster  $M/L$ , the 2% statistical error in the mean luminosity density, and our estimated 10% systematic error in the normalization of equation (10), but we have not considered other possible sources of systematic error. We find similar results comparing to the  $M/L$  ratios of SDSS clusters inferred from Bahcall et al. (2003a) or to the  $M/L$  ratios of the virial regions of clusters found by Rines et al. (2004), but the systematic uncertainties are larger and harder to quantify because of our reliance on mean scaling relations in the former case and the complications of passband and geometry conversions in the latter. If we used the Rines et al. (2004)  $M/L$  estimates from cluster infall regions, we would infer a somewhat lower value of  $\sigma_8 \Omega_m^{0.6}$ .

Our estimate (12) derived from cluster mass-to-light ratios conflicts with recent estimates obtained by combining CMB anisotropy measurements with the large scale galaxy power spectrum, Type Ia supernova data, the Ly $\alpha$  forest flux power spectrum, and weak gravitational lensing, which tend to favor  $\sigma_8 \approx 0.9$ ,  $\Omega_m \approx 0.3$  (e.g., Spergel et al. 2003; Tegmark et al. 2004; Seljak et al. 2004). For example, Seljak et al. (2004) quote  $\sigma_8 = 0.897_{-0.031}^{+0.033}$ ,  $\Omega_m = 0.281_{-0.021}^{+0.023}$  as their combined constraint for a 6-parameter, spatially flat  $\Lambda$ CDM model, corresponding to  $\sigma_8 \Omega_m^{0.6} = 0.419 \pm 0.026$ . Our conclusion agrees well with that of van den Bosch et al. (2003), who find that “concordance” values of  $\sigma_8 = 0.9$ ,  $\Omega_m = 0.3$  are favored by their conditional luminosity function analyses of the 2dFGRS only for cluster mass-to-light ratios of  $750 h M_\odot/L_\odot$ . If they impose a more observationally plausible constraint of  $(M/L)_{\text{cl}} = 350 \pm 70 h M_\odot/L_\odot$  (in  $b_J$ -band), they find  $\Omega_m = 0.25_{-0.07}^{+0.10}$  and  $\sigma_8 = 0.78 \pm 0.12$ , in good agreement with equation (12). Although our calculation is similar in overall concept to van den Bosch et al.’s, we parameterize the problem in a completely different way, fit different constraints in a different order, use different approximations, and analyze measure-

ments from an independent galaxy redshift survey, red-selected instead of blue-selected. In contrast to our fixed linear  $P(k)$ , van den Bosch et al. (2003) vary the power spectrum shape parameter linearly with  $\Omega_m$ . The agreement of the two results is therefore a good indication that the conclusions are robust to details of the measurements or analysis procedures.

Equation (12) is nearly identical to the constraint  $\sigma_8\Omega_m^{0.6} = 0.33 \pm 0.03$  obtained by Bahcall et al. (2003b) in their analysis of the mass function of clusters in the SDSS Early Data Release. Earlier analyses of cluster mass functions have generally yielded higher normalizations of this constraint (e.g., White et al. 1993; Eke et al. 1996; Bahcall & Fan 1998; Henry 2000). While the mass function and mass-to-light ratio methods both incorporate cluster masses, they are physically distinct: the former has no dependence on galaxy luminosities, and the latter uses an average mass and is therefore insensitive to scatter in observational estimates. Low values of  $\sigma_8$  or  $\Omega_m$  would also help explain observational estimates of the galaxy pairwise velocity distribution, which appear to conflict with predicted values for  $\sigma_8 = 0.9$ ,  $\Omega_m = 0.3$  (Yang et al. 2004).

Our HOD modeling assumes that satellite galaxies in halos have a radial profile corresponding to an NFW model with the concentration predicted for  $\Omega_m = 0.3$ . To test our sensitivity to this assumption, we lower all of the assumed halo concentrations in the  $\sigma_8 = 0.9$  model by 30% and refit  $w_p(r_p)$ , which results in slightly different  $P(N|M)$  and thus slightly different  $M/L$ . We find a 1.8% difference in  $(M/L)_{\text{cl}}$  for this HOD model, so radial profiles are not an important source of systematic uncertainty. As noted in §2, changing the assumed linear matter power spectrum from the Efstathiou et al. (1992) parameterization to a CMBFAST calculation makes a significant difference to the  $\chi^2$  values of  $w_p(r_p)$  fits but minimal change to the HOD parameters themselves, so our  $M/L$  predictions are not sensitive to modest changes in the power spectrum shape. The main source of systematic uncertainty in our  $(M/L)_{\text{cl}}$  predictions is therefore the 10% uncertainty associated with the HOD parameterization and the  $w_p(r_p)$  measurements, discussed at the end of §2 (see Fig. 4).

Turning to the observational uncertainties, cluster  $M/L$  ratios could be underestimated if masses are biased low or luminosities are biased high. Cluster mass estimation is a challenging problem, but the generally good agreement between virial mass estimates, Jeans equation estimates, and estimates from X-ray or weak lensing data (see Bahcall & Comerford [2002] and references therein) argues against a systematic error as large as a factor of  $588/359 = 1.64$ , the ratio of our predicted  $M/L$  for  $\Omega_m = 0.3$ ,  $\sigma_8 = 0.9$  to Carlberg et al.’s (1996) observational estimate. Luminosities could be biased high if background subtraction methods do not adequately account for overdense structures surrounding clusters, an issue that warrants further investigation with realistic mock galaxy catalogs. We see no obvious

holes in the CMB + large scale structure analyses, but in contrast to the approach taken here and in van den Bosch et al. (2003), these methods of inferring cosmological parameters rely on a detailed theoretical model of primordial fluctuations and their linear evolution, and they are sensitive to quantities like the electron scattering optical depth, the CMB tensor-to-scalar ratio, and the curvature of the inflationary fluctuation spectrum.

At present, it seems plausible that the results of these different methods can be reconciled without major revisions, if  $\sigma_8$  and  $\Omega_m$  lie at the low end of the ranges allowed by Tegmark et al. (2004) or Seljak et al. (2004), cluster  $M/L$  ratios are somewhat higher than the estimates shown in Figures 6 and 8, and our HOD parameterization leads to a modest over-prediction of  $M/L$  for a given  $\sigma_8$  and  $\Omega_m$ . Fortunately, the remaining uncertainties can be substantially reduced in the near future. The SDSS redshift survey is now large enough that rich clusters can be identified directly from the redshift survey itself, reducing (though not eliminating) problems of contamination and background subtraction. Follow-up observations of these systems can provide consistency checks of mass estimates via galaxy dynamics, X-ray modeling, and weak lensing. The HOD parameter constraints can be greatly improved by bringing in additional clustering measurements, most notably the group multiplicity function (A. Berlind et al., in preparation) and the projected three-point correlation function. Redshift-space distortion analysis can yield independent constraints on  $\sigma_8$  and  $\Omega_m$ . Advances on all of these fronts should soon show whether the current tension in parameter estimates arises from an accumulation of systematic errors or instead signals the need for a new physical ingredient in the standard cosmological scenario.

We thank Frank van den Bosch, Risa Wechsler, and Jaiyul Yoo for helpful discussions. This work was supported by NSF Grant AST-0407125. JT acknowledges the support of a Distinguished University Fellowship at Ohio State University, and ZZ acknowledges the support of NASA through Hubble Fellowship grant HF-01181.01-A awarded by the Space Telescope Science Institute, which is operated by the Association of Universities for Research in Astronomy, Inc., for NASA, under contract NAS 5-26555. The simulations were performed on the Beowulf and Itanium clusters at the Ohio Supercomputing Center under grants PAS0825 and PAS0023. Funding for the creation and distribution of the SDSS Archive has been provided by the Alfred P. Sloan Foundation, the Participating Institutions, the National Aeronautics and Space Administration, the National Science Foundation, the U.S. Department of Energy, the Japanese Monbukagakusho, and the Max Planck Society. The Participating Institutions are listed at the SDSS web site, <http://www.sdss.org>.

## A. Halo and Galaxy Bias

Halo clustering is biased relative to that of the underlying mass distribution, by an amount that depends on halo mass. Halo bias factors are an important ingredient in analytic calculations of galaxy clustering, including those in this paper. Following the pioneering work of Mo & White (1996), a number of authors have investigated halo bias using N-body simulations (e.g., Porciani et al. 1999; Sheth & Lemson 1999; Sheth & Tormen 1999; Jing 1998, 1999; Sheth, Mo, & Tormen 2001). However, many of these studies are based on simulations of either low mass resolution or limited box size (the main exception is the recent study of Seljak & Warren [2004], which we discuss below). Most previous studies have also compared different cosmologies such as open and standard CDM to one version of  $\Lambda$ CDM, rather than focusing on variants of the  $\Lambda$ CDM cosmology with a wide range of  $\sigma_8$  as we have done here. We have also performed an identical set of simulations with a power spectrum shape parameter of  $\Gamma = 0.12$ , which significantly increases the large-scale power and reduces the power on small scales relative to our standard choice of  $\Gamma = 0.2$ . Our simulations are therefore well suited to investigate halo bias for the cosmological models of the greatest interest today, and to investigate the dependence of bias factors on power spectrum shape or normalization. The use of five realizations and a reasonably large volume ( $253 h^{-1}$  Mpc on a side) yields good statistics for high mass halos. Note that we define halos using a friends-of-friends algorithm with linking length  $l = 0.2n^{-1/3}$ . Alternative definitions would yield slightly different halo masses (see Hu & Kravtsov 2003) and would therefore require a slightly different formula for  $b_h(M)$ .

The halo bias factor can be defined by the ratio of halo and mass autocorrelations, or power spectra, or using the halo–mass cross-correlation. Since we are interested in modeling galaxy autocorrelations, we adopt the definition  $b_h^2(M) = \xi_h(r, M)/\xi_m(r)$ , where  $\xi_h(r, M)$  is the autocorrelation function of halos of mass  $M$  and  $\xi_m(r)$  is the non-linear matter correlation function measured from the simulations. Sheth et al. (2001, hereafter SMT) give an analytic formula for  $b_h$ , motivated by the analytic model of Sheth & Tormen (1999) but empirically calibrated against numerical simulations:

$$b_h(\nu) = 1 + \frac{1}{\sqrt{a}\delta_c} \left[ \sqrt{a}(a\nu^2) + \sqrt{ab}(a\nu^2)^{1-c} - \frac{(a\nu^2)^c}{(a\nu^2)^c + b(1-c)(1-c/2)} \right], \quad (\text{A1})$$

where  $\delta_c = 1.686$  is the critical overdensity required for collapse and  $\nu = \delta_c/\sigma(M)$ , with  $\sigma(M)$  the linear theory rms mass fluctuation in spheres of radius  $r = (3M/4\pi\bar{\rho})^{1/3}$ . The three parameters in this equation are  $a = 0.707$ ,  $b = 0.5$ , and  $c = 0.6$ , as listed in SMT.

We divide the halos in our simulations into bins separated by factors of two in mass. The

logarithmic center of the lowest bin is  $1.22 \times 10^{12} (\Omega_m/0.3) h^{-1} M_\odot$ , below  $M_*$  for  $\sigma_8 > 0.6$ . We calculate halo bias by averaging  $\sqrt{\xi_h/\xi_m}$  for radii  $4 \leq r \leq 12 h^{-1} \text{Mpc}$ , a regime in which the ratio of the halo and matter correlation functions is approximately constant and noise is not a factor. The results are plotted in Figure 10. The dashed line, which shows the SMT bias relation, is significantly higher than the values of  $b_h$  calculated from the simulations for both values of  $\Gamma$ . A better fit to the calculations is shown with the solid line, which plots a bias relation of the same form as equation (A1), but with  $a = 0.707$ ,  $b = 0.35$ , and  $c = 0.80$ . With these parameter values, the formula gives accurate fits to our numerical results for the full range of  $\sigma_8$  values, and it works equally well for  $\Gamma = 0.2$  and  $\Gamma = 0.12$ . Increasing either the lower or upper bounds of the radial range over which  $b_h$  is calculated does not appreciably change the bias values or the quality of the fits.

The inset box in Figure 10 plots an example of using equation (9) to calculate the galaxy bias with our modified parameters of equation (A1), which we compare to the galaxy bias in the simulations calculated by the same method as the halo bias for five values of  $\sigma_8$ . The plot symbols represent the galaxy bias calculated from the simulations, and the solid lines represent the analytic calculations (eq. [9]) using equation (A1) with our new parameters. For this test, the HOD parameters used to populate the simulations are taken from Table 1 of Tinker et al. (2005), parameters similar to the  $M_r < -20$  sample. The analytically calculated bias factors differ from the simulation results by  $\lesssim 1\%$ .

Recently Seljak & Warren (2004, hereafter SW) proposed a new empirically determined halo bias relation, empirically calibrated on large simulations (up to  $768^3$  particles) with cosmological parameters close to the best-fit values from CMB and large-scale structure measurements. The dotted line in Figure 10 shows the SW formula evaluated for  $\Gamma = 0.2$  and  $\sigma_8 = 0.9$ , which fits our numerical data accurately. However, the SW formula is expressed in terms of  $M/M_*$ , where  $\sigma(M_*) = \delta_c$ , instead of  $\nu = \delta_c/\sigma(M)$ , and the mapping between  $M/M_*$  and  $\nu$  depends on the amplitude and shape of the power spectrum. We find that the SW formula becomes a poor fit to our results at low  $\sigma_8$ , and the discrepancies are worse for  $\Gamma = 0.12$ , as illustrated in the inset box by calculating the galaxy bias parameters with the SW halo bias formula. Thus, their formula is accurate for models close to the cosmological concordance model, but our modified version of the SMT formula, with  $\nu$  as the halo mass parameter, applies more universally.

We have not investigated alternative definitions of bias using the power spectrum or mass cross-correlation, or using linear instead of non-linear matter clustering. We also note that our numerical results do not extend much below  $\nu = 1$ , and simulations of smaller volumes or larger dynamic range are needed to test equation (A1) in the low mass regime.

## B. The Analytic Model

Our analytic calculation of the two-point galaxy correlation function is similar to that presented by Zheng (2004) and used in Zehavi et al.’s (2004a,b) modeling of the SDSS  $w_p(r_p)$ . Here we report improvements in the procedure that have been incorporated in our present analysis. For completeness and clarity, we describe the method from start to finish. The new ingredients are the use of the modified halo bias formula of Appendix A and the more accurate treatment of halo exclusion described by equations (B10) and (B12). The Zheng (2004) procedure was calibrated and tested using the 144  $h^{-1}$  Mpc, 256<sup>3</sup> particle GIF simulation of Jenkins et al. (1998), which was also used to calibrate the SMT formula. Our use of the five 253  $h^{-1}$  Mpc, 360<sup>3</sup> particle simulations described in §3 allows us to achieve a more accurate calibration and to test the procedure for a range of cosmological parameters.

The correlation function is defined as the probability above random of there being a pair of objects at separation  $r$ . In the HOD context, a pair of galaxies can reside within a single halo or come from two distinct halos. These two contributions are computed separately and combined to get the full correlation function, i.e.

$$\xi(r) = [1 + \xi_{1h}(r)] + \xi_{2h}(r). \quad (\text{B1})$$

The “1+” arises because it is the pair counts, proportional to  $1 + \xi_{1h}$  and  $1 + \xi_{2h}$ , that sum to give the total pair counts, proportional to  $1 + \xi$ . The one-halo term is calculated in real space through (Berlind & Weinberg 2002)

$$1 + \xi_{1h}(r) = \frac{1}{2\pi r^2 \bar{n}_g^2} \int_0^\infty dM \frac{dn}{dM} \frac{\langle N(N-1) \rangle_M}{2} \frac{1}{2R_{\text{vir}}(M)} F' \left( \frac{r}{2R_{\text{vir}}} \right), \quad (\text{B2})$$

where  $\bar{n}_g$  is the mean number density of galaxies,  $dn/dM$  is the halo mass function (Sheth & Tormen 1999; Jenkins et al. 2001), and  $\langle N(N-1) \rangle_M/2$  is the average number of pairs in a halo of mass  $M$ . The function  $F(x)$  is the average fraction of galaxy pairs in a halo of mass  $M$  (or virial radius  $R_{\text{vir}}$ ) that have separation less than  $r$ , which is related to the halo density profile,  $\rho_m(r)$ , and  $F'(x)$  is its derivative. In practice,  $F(x)$  must be treated differently for central-satellite galaxy pairs and satellite-satellite pairs. In the former, the pair distribution is proportional to the volume-weighted density profile,  $F'(x) \propto \rho_m(r)r^2$ , normalized to one. For the latter it is derived from the halo profile convolved with itself, a calculation that can be done analytically for an NFW profile (Sheth et al. 2001). The average number of one-halo pairs in the range  $(x, x + dx)$  in halos of mass  $M$  can be written explicitly as

$$\frac{\langle N(N-1) \rangle_M}{2} F'(x) dx = \langle N_{\text{cen}} N_{\text{sat}} \rangle_M F'_{\text{cs}}(x) dx + \frac{\langle N_{\text{sat}}(N_{\text{sat}}-1) \rangle_M}{2} F'_{\text{ss}}(x) dx, \quad (\text{B3})$$

where the subscripts *cs* and *ss* refer to central-satellite pairs and satellite-satellite pairs respectively. For a Poisson distribution of satellite occupation,  $\langle N_{\text{sat}}(N_{\text{sat}}-1) \rangle = \langle N_{\text{sat}} \rangle^2$ . We use an NFW profile with concentration parameters as a function of halo mass calculated by the method of Bullock et al. (2001) and Kuhlen et al. (2004).

The one-halo term dominates  $\xi_g(r)$  at small scales, while the two-halo term fully accounts for all galaxy pairs at separations  $\gtrsim 5 h^{-1}$  Mpc. The transition region between one-halo and two-halo dominance is difficult to model because only certain regions of the halo mass function can contribute to the two-halo term at small scales. The range of halo masses included must ensure that halo pairs do not overlap, since such halo pairs would be merged into a single halo by the friends-of-friends scheme that we use to define halos in the first place. It is this one-halo to two-halo transition that causes  $w_p(r_p)$  to deviate from a power-law at scales near  $1 h^{-1}$  Mpc (Zehavi et al. 2004a,b); as  $r$  increases,  $\xi_{1h}$  drops rapidly, while the rise in  $\xi_{2h}$  is regulated by halo exclusion. For brighter galaxies, which preferentially occupy high-mass halos, the rise in  $\xi_{2h}$  occurs at a larger  $r$ , making the deviation from a power-law greater for brighter galaxy samples.

Since the radial distribution of galaxies within halos must be accounted for in the calculation of the two-halo term, the calculation itself is done in Fourier space, where the convolutions with the halo density profile become multiplications instead (Scherrer & Bertschinger 1991; Seljak 2000; Soccimarro et al. 2001). In the method of Zheng (2004), halo exclusion was treated by only including halos with virial radii less than half the value of  $r$  for which  $\xi_g(r)$  is being calculated, i.e. with masses below

$$M_{\text{lim}} = \frac{4}{3} \pi \left( \frac{r}{2} \right)^3 \rho_{\text{crit}} \Omega_m \Delta, \quad (\text{B4})$$

where  $\Delta$  is the virial overdensity of the halo, relative to the mean density, which we have chosen to be 200. With this implementation of halo exclusion, the calculation of the two-halo term in Fourier space is

$$P_{\text{gg}}^{2h}(k, r) = P_m(k) \left[ \frac{1}{\bar{n}'_g} \int_0^{M_{\text{lim}}} dM \frac{dn}{dM} \langle N \rangle_M b_h(M, r) y_g(k, M) \right]^2, \quad (\text{B5})$$

where  $y_g(k, M)$  is the Fourier transform of the halo density profile (e.g. Cooray & Sheth

2002),  $b_h(M, r)$  is the halo bias at separation  $r$ , and the restricted number density  $\bar{n}'_g$  is the average number density of galaxies that reside in halos with  $M \leq M_{\text{lim}}$ ,

$$\bar{n}'_g = \int_0^{M_{\text{lim}}} dM \frac{dn}{dM} \langle N \rangle_M. \quad (\text{B6})$$

The matter power spectrum,  $P_m(k)$ , is the non-linear form given by Smith et al. (2003). At large  $r$ , equation (B5) can be thought of as simply multiplying the non-linear matter power spectrum by the galaxy pair-weighted halo bias factor to obtain the galaxy power spectrum. At smaller separations the finite size of the halos must be taken into account. The scale dependence of halo bias also becomes important at  $r \lesssim 3 h^{-1} \text{Mpc}$ . Parameterizing the scale dependence by the amplitude of the non-linear matter correlation function, the scale dependence of halo bias is well described by

$$b^2(M, r) = b^2(M) \frac{[1 + 1.17 \xi_m(r)]^{1.49}}{[1 + 0.69 \xi_m(r)]^{2.09}}, \quad (\text{B7})$$

where  $b(M)$  is the large-scale bias, for which we have used the bias relation given in Appendix A. Equation (B7), determined from inspection of our numerical simulations, is fairly accurate for the full range of  $\sigma_8$  values and both values of  $\Gamma$  explored in this paper.

At a given  $r$ , equation (B5) is solved for all  $k$ , then converted to real space by

$$\xi'_{2\text{h}}(r) = \frac{1}{2\pi^2} \int_0^\infty P_{\text{gg}}^{2\text{h}}(k, r) k^2 \frac{\sin kr}{kr} dk, \quad (\text{B8})$$

where  $\xi'_{2\text{h}}(r)$  denotes that we have calculated the two-halo term for a restricted range of the halo mass function. The value calculated in equation (B8) is converted to a probability over random for the entire halo (and therefore galaxy) population by

$$1 + \xi_{2\text{h}}(r) = \left( \frac{\bar{n}'_g}{\bar{n}_g} \right)^2 [1 + \xi'_{2\text{h}}(r)]. \quad (\text{B9})$$

The virtue of this implementation is that the integral over mass in equation (B5) is calculated once and squared, instead of being a double integral over different halo pairs. This approximation, however, neglects galaxy pairs from halos larger than  $M_{\text{lim}}$  paired with smaller halos. In Figure 11, we compare this analytic method to numerical results. For this comparison we use the correlation functions calculated from the N-body simulations described in §3, but following Tinker et al.'s (2004) practice of drawing satellite galaxy

populations from the appropriate NFW profile instead of randomly sampling the friends-of-friends dark matter distribution, as done in §3. We use the  $\sigma_8 = 0.8$  output with HOD parameters  $M_{\min} = 1.11 \times 10^{12}$ ,  $M_1 = 2.53 \times 10^{13}$ , and  $\alpha = 1.01$ .

Figure 11a compares the N-body two-halo term to equation (B9) calculated both with our new halo bias parameters and with the original parameters of the SMT function. At  $r \gtrsim 10 h^{-1}$  Mpc, the original SMT relation over-predicts the galaxy bias by  $\sim 15\%$  and the correlation function by  $\sim 30\%$ . The new bias function yields an excellent match at these scales. At smaller scales, this method of halo exclusion under-predicts the number of two-halo pairs, with errors greater than 50% at  $1 h^{-1}$  Mpc. Although the one-halo term begins to dominate at this scale, the large error in  $\xi_{2h}$  is still apparent in the total correlation function, shown in panel (b). The  $\sim 5\%$  error at the smallest scales is due to the fact that the halo mass function of our simulations is not precisely represented by the Jenkins et al. (2001) function assumed in the analytic calculation. The two-halo term is much less sensitive to the mass function, and is not affected by this difference.

The numerical test in the Appendix of Zehavi et al. (2004a) showed a much smaller discrepancy on large scales because the  $144 h^{-1}$  Mpc GIF simulation used for the test (and for the calibration of the SMT bias factors) has a high amplitude of large scale clustering for low mass halos. With our multiple, larger volume simulations, the need for lower halo bias factors is evident, and these in turn drive the need for a more accurate treatment of halo exclusion. Zehavi et al. (2004a,b) find a low  $\chi^2/\text{d.o.f.}$  fitting the projected correlation function of luminous,  $M_r \leq -21$  galaxies, while we find a relatively high  $\chi^2/\text{d.o.f.}$  for this sample (see Table 1). However, as noted in §2, the  $\chi^2$  values of  $w_p(r_p)$  fits are sensitive to the difference between a  $\Gamma = 0.2$  power spectrum and a (presumably more realistic) CMBFAST power spectrum, even though the best-fit HOD parameters are not. Combination of our present  $\xi_g(r)$  calculation with the CMBFAST power spectrum produces a similar  $w_p(r_p)$  for  $M_r \leq -21$  galaxies, with similarly low  $\chi^2$ , to that obtained with the Zheng (2004) prescription and a  $\Gamma = 0.2$  power spectrum. Thus, this more accurate modeling leads to the same bottom line conclusion as Zehavi et al. (2004a,b), and similar HOD parameters.

We now return to the halo exclusion problem. Under the assumption of spherical halos, all two-halo pairs would be accounted for by summing all the galaxies from halo pairs for which the sum of virial radii is smaller than the separation, i.e.  $R_{\text{vir}1} + R_{\text{vir}2} \leq r$ . For this “spherical halo” exclusion, equation (B5) must be modified to

$$P_{\text{gg}}^{2h}(k, r) = P_m(k) \frac{1}{\bar{n}_g'^2} \int_0^{M_{\text{lim},1}} dM_1 \frac{dn}{dM_1} \langle N \rangle_{M_1} b_h(M_1, r) y_g(k, M_1)$$

$$\int_0^{M_{\text{lim},2}} dM_2 \frac{dn}{dM_2} \langle N \rangle_{M_2} b_h(M_2, r) y_g(k, M_2), \quad (\text{B10})$$

where  $M_{\text{lim},1}$  is the maximum halo mass such that  $R_{\text{vir}}(M_{\text{lim},1}) = r - R_{\text{vir}}(M_{\text{min}})$  and  $M_{\text{lim},2}$  is related to  $M_1$  by  $R_{\text{vir}}(M_{\text{lim},2}) = r - R_{\text{vir}}(M_1)$ . Since the upper limit of the second integral depends on the integrand of the first, equation (B10) must be solved as a double integral, making it more computationally expensive than equation (B5), but significantly more accurate by increasing the number of small-separation two-halo pairs counted.

The range of halo masses over which the two-halo term is calculated is different than that in equation (B5), and the restricted number density  $\bar{n}'_g$  must reflect that change. Using this new method of halo exclusion,  $\bar{n}'_g$  becomes

$$\bar{n}'_g{}^2 = \int_0^{M_{\text{lim},1}} dM_1 \frac{dn}{dM_1} \langle N \rangle_{M_1} \int_0^{M_{\text{lim},2}} dM_2 \frac{dn}{dM_2} \langle N \rangle_{M_2}. \quad (\text{B11})$$

Figures 11c and 11d compare our numerical results to the spherical exclusion method. At  $r = 1 h^{-1}$  Mpc, where the previous method resulted in a  $\sim 50\%$  error, the error has been reduced to  $\sim 25\%$ . At  $r = 2 h^{-1}$  Mpc, the  $\sim 20\%$  error in the previous method is eliminated entirely.

Halos are not spherical objects, however. They are triaxial objects that can exhibit significant flattening (see, e.g. Jing & Suto 2002). This can lead to halo pairs which are closer than the sum of their virial radii. By assuming a lognormal distribution of ellipticities with mean flattenings motivated by simulation results, one can determine the probability that halos of a given separation are allowed. This probability,  $P(x)$ , where  $x = r/(R_{\text{vir}1} + R_{\text{vir}2})$ , can be used to modify the two-halo calculation to

$$P_{\text{gg}}^{2\text{h}}(k, r) = P_m(k) \frac{1}{\bar{n}'_g{}^2} \int_0^\infty dM_1 \frac{dn}{dM_1} \langle N \rangle_{M_1} b_h(M_1, r) y_g(k, M_1) \int_0^\infty dM_2 \frac{dn}{dM_2} \langle N \rangle_{M_2} b_h(M_2, r) y_g(k, M_2) P(x), \quad (\text{B12})$$

where the limits in equation (B12) are both infinity (but in practice can be cut off at some reasonably large value) but the calculation is still a double integral because the value of  $M_1$  is used in the ellipsoidal exclusion probability in the integral over  $M_2$ .

We investigated the ellipsoidal exclusion probability by a Monte Carlo approach. We assume a lognormal distribution of halo axis ratios  $q$  with dispersion 0.2 and means  $q_b =$

$b/a = 0.9$  and  $q_c = c/a = 0.8$ , motivated by the results of Jing & Suto (2002), then assume the axis ratios have a lognormal distribution in  $q$  with a dispersion of 0.2. By randomly selecting ellipticities and orientation angles for halos of a given mass ratio and separation, we find that the probability of non-overlapping halos is well approximated by  $P(y) = (3y^2 - 2y^3)$  in the range  $0 \leq y \leq 1$ , where  $y = (x - 0.8)/0.29$ . At  $y < 0$ ,  $P(y) = 0$ , and at  $y > 1$ ,  $P(y) = 1$ . The restricted number density,  $\bar{n}'_g$ , must also be calculated in this way. Equation (B6) becomes

$$\bar{n}'_g{}^2 = \int_0^\infty dM_1 \frac{dn}{dM_1} \langle N \rangle_{M_1} \int_0^\infty dM_2 \frac{dn}{dM_2} \langle N \rangle_{M_2} P(x). \quad (\text{B13})$$

The results of the ellipsoidal halo exclusion are presented in panels (c) and (d) of Figure 11. The ellipsoidal exclusion approach is an improvement over spherical exclusion; at  $r = 1 h^{-1}$  Mpc, the error in the two-halo term has been reduced to  $\sim 10\%$ . Choosing more extreme values of  $q_b$  and  $q_c$  does not significantly change the results. This ellipsoidal exclusion method is the one we have used for the calculations in this paper.

Although this approach is more accurate, the added computation time can become prohibitive when fitting observed data to high precision, where many hundreds of iterations are required. We have therefore created a halo exclusion approach that mimics the results of ellipsoidal exclusion but can be written as separable integrals in the Fourier-space calculation of  $P_{\text{gg}}^{2\text{h}}(k, r)$ . Although the evaluation of equation (B12) is CPU intensive, the calculation of the restricted number density under the ellipsoidal approach is relatively rapid. For a more efficient scheme, we recalculate the ellipsoidal  $\bar{n}'_g$  first, and then  $M_{\text{lim}}$  in equation (B6) is increased until the restricted number density matches that of the ellipsoidal calculation. We then use equation (B5) to calculate  $\xi_{2\text{h}}$ .

The results of this approximation, which we call  $\bar{n}'_g$ -matched, are shown in panels (c) and (d) of Figure 11. The loss of accuracy relative to the full ellipsoidal treatment is minimal. In further tests with multiple values of  $\sigma_8$  and HOD parameters that give higher and lower galaxy space densities, we find similar results.

Although the methods introduced here significantly improve the analytic calculation of  $\xi_g(r)$  for specified cosmological and HOD parameters, there is room for further investigation and improvement. Outstanding issues include the small but non-negligible dependence of the halo mass function shape on cosmology (i.e., the non-universality of the Jenkins et al. [2004] formula), the effect of scatter in concentrations and halo ellipticity on the one-halo term, bias factors of low mass halos, effects of cosmology on the scale-dependence of halo bias, the dependence of the approximation on the halo definition, and the interaction of all of these effects with the treatment of halo exclusion. We are presently investigating a

number of these issues. The long-term goal is to ensure that errors in the calculation of  $\xi_g(r)$  for specified parameters are a negligible source of uncertainty in the inference of HOD and cosmological parameters from observational data. Because of the high precision of the clustering measurements, it is not clear that we have yet reached this goal.

## REFERENCES

- Abell, G. O. 1958, *ApJS*, 3,211
- Berlind, A. A., & Weinberg, D. H. 2002, *ApJ*, 575, 587
- Berlind, A.A., Weinberg, D.H., Benson, A.J., Baugh, C.M., Cole, S., Davé, R., Frenk, C.S., Katz, A., & Lacey, C.G. 2003, *ApJ*, 593, 1
- Bahcall, N. A., Lubin, L. M., & Dorman, V. 1995, *ApJ*, 447, 81
- Bahcall, N. A., & Fan, X. 1998, *ApJ*, 504, 1
- Bahcall, N. A., Cen R., Davé, R., Ostriker, J. P., & Yu, Q. 2000, *ApJ*, 541, 1 (B00)
- Bahcall, N. A. & Comerford J. N. 2002, *ApJ*, 565, L5
- Bahcall, N. A., et al. 2003a, *ApJS*, 148, 243
- Bahcall, N. A., et al. 2003b, *ApJ*, 585, 182
- Benson, A. J., Cole, S., Frenk, C. S., Baugh, C. M., & Lacey, C. G. 2000, *MNRAS*, 311, 793
- Blanton, M. R., et al. 2003, *ApJ*, 592, 819
- Bullock, J. S., Kolatt, T. S., Sigad, Y., Somerville, R. S., Klypin, A. A., Primack, J. R., Dekel, A. 2001, *MNRAS*, 321, 559
- Carlberg, R. G., Yee, H. K. C., Ellingson, E., Abraham, R., Gravel, P., Morris, S., Pritchett, C. J. 1996, *ApJ*, 462, 32
- Carlberg, R. G., Yee, H. K. C., Ellingson, E. 1997, *ApJ*, 478, 462
- Colless, M. et. al. 2001, *MNRAS*, 328, 1039
- Collister, A. A., & Lahav, O. 2004, *MNRAS* (submitted), astro-ph/0412516
- Cooray, A. & Sheth, R. K. 2002, *Phys. Rep.*, 372, 1

- Diaferio, A. & Geller, M. J. 1997, *ApJ*, 481, 633
- Diaferio, A. 1999, *MNRAS*, 309, 610
- Efstathiou, G., Bond, J. R., & White, S. D. M. 1992, *MNRAS*, 258, 1
- Eke, V. R., Cole, S., & Frenk, C. S. 1996, *MNRAS*, 282, 263
- Eke, V. R., et al. 2004, *MNRAS*, 348, 866
- Evrard, A. E., Metzler, C. M. & Navarro, J. F. 1996, *ApJ*, 469, 494
- Gott, J. R., Schramm, D. N., Tinsley, B. M., & Gunn, J. E. 1974, *ApJ*, 194, 543
- Hansen, S. H., McKay, T. A., Annis, J., Wechsler, R. H., Sheldon, E. S., & Kimball, A. 2004, *ApJ* (submitted), astro-ph/0410467
- Henry, J. P. 2000, *ApJ*, 534, 565
- Hu, W. & Kravtsov, A.V., 2003, *ApJ*, 584, 702
- Jenkins, A., Frenk, C. S., Pearce, F. R., Thomas, P. A., Colberg, J. M., White, S. D. M., Couchman, H. M. P., Peacock, J. A., & Efstathiou, G., & Nelson, A. H. 1998, *ApJ*, 499, 20
- Jing, Y.P. 1998, *ApJ*, 376, L9
- Jing, Y.P. 1999, *ApJ*, 515, L45
- Jing, Y. P., Mo, H. J., & Börner, G. 1998, *ApJ*, 494, 1
- Jing, Y. P., & Suto, Y. 2002, *ApJ*, 574, 538
- Jenkins, A., Frenk, C. S., White, S. D. M., Colberg, J. M., Cole, S., Evrard, A. E., Couchman, H. M. P., & Yoshida, N. 2001, *MNRAS*, 321, 372
- Kauffmann, G., Nusser, A., & Steinmetz, M. 1997, *MNRAS*, 286, 795
- Kauffmann, G., Colberg, J. M., Diaferio, A., White, S. D. M. 1999, *MNRAS*, 303, 188
- Kochanek, C. S., White, M., Huchra, J., Macri, L., Jarrett, T. H., Schneider, S. E., & Mader, J. 2003, *ApJ*, 585, 161
- Kravtsov, A. V., Berlind, A. A., Wechsler, R. H., Klypin, A. A., Gottlöber, S., Allgood, B., Primack, J. R. 2004, *ApJ*, 609, 35

- Kuhlen, M., Strigari, L. E., Zentner, A. R., Bullock, J. S., Primack, J. R., 2005, MNRAS, 357, 873
- Lewis, A., & Bridle, S. 2002, Phys. Rev. D, 66, 3511
- Lin, Y.-T., Mohr, J. J., & Stanford, S. S. 2003, ApJ, 591, 749
- Lin, Y.-T., Mohr, J. J., & Stanford, S. S. 2004, ApJ, 610, 745
- Mo, H. J., & White, S. D. M. 1996, MNRAS, 282, 1096
- Mo, H. J., Yang, X., & van den Bosch, F. C. 2004, MNRAS, 349, 205
- Navarro, J. F., Frenk, C. S., & White, S. D. M. 1997, ApJ, 490, 493
- Pahre, M. A. 1999, ApJS, 124, 127
- Peebles, P. J. E. 1986, Nature, 321, 27
- Percival, W. J. et al. 2002, MNRAS, 337, 1068
- Popesso, P., Biviano, A., Boehringer, H., Romaniello, M., & Voges, W. 2005, A&A, 433, 431
- Porciani, C., Catelan, P., & Lacey, C. 1999, ApJ, 513, L99
- Rines, K., Geller, M. J., Diaferio, A., Kurtz, M. J., & Jarrett, T. H. 2004, AJ, 128, 1078
- Rines, K., Geller, M. J., Kurtz, M. J., & Diaferio, A. 2004, AJ, 128, 1078
- Scherrer, R. J. & Bertschinger, E. 1991, ApJ, 381, 349
- Scoccimarro, R., Sheth, R. K., Hui, L., Jain, B. 2001, ApJ, 546, 205
- Seljak, U., 2000, MNRAS, 318, 203
- Seljak, U. et al., 2004, ApJ (submitted), astro-ph/0407372
- Seljak, U., & Warren, M. S. 2004, MNRAS, 355, 129
- Seljak U. & Zaldarriaga M. 1996, ApJ, 469, 437
- Sheth, R. K. & Tormen, G. 1999, MNRAS, 308, 119
- Sheth, R. K. & Lemson, G. 1999, MNRAS, 304, 767
- Sheth, R. K., Mo, H. J., & Tormen, G. 2001, MNRAS, 323, 1

- Sheth, R. K., Hui, L., Diaferio, A., & Scoccimarro, R. 2001, MNRAS, 325, 1288
- Smith R. E., et al. 2003, MNRAS, 341, 1311
- Spergel, D.N., et al. 2003, ApJ, 148, 175
- Springel, V., Yoshida, N., & White, S. D. M. 2001 NewA, 6, 79
- Tegmark, M., et al. 2004, ApJ, 606, 702
- Tinker, J. L., Weinberg, D. H., & Zheng, Z. 2005, MNRAS (submitted), astro-ph/0501029
- Turner, M. L. 2002, ApJ, 517, 101L
- van den Bosch, F. C., Yang, X., & Mo, H. J. 2003, MNRAS, 345, 723
- Wechsler, R. H. et al. 2004, in preparation for submission to ApJ
- White, S. D. M., Efstathiou, G., & Frenk, C. S. 1993, MNRAS, 262, 1023
- White, M., Hernquist, L., & Springel, V. 2001, ApJ, 550, L129
- Yang, X. H., Mo, H. J., & van den Bosch, F. C. 2003, MNRAS, 339, 1057
- Yang, X., Mo, H. J., Jing, Y. P., van den Bosch, F. C., & Chu, X. Q. 2004, MNRAS, 350, 1153
- York, D. et al. 2000, AJ, 120, 1579
- Yoshikawa, K., Taruya, A., Jing, Y.P., & Suto, Y. 2001, ApJ, 558, 520
- Zehavi, I., Weinberg, D. H., Zheng, Z., Berlind, A. A., Frieman, J. A., et al. 2004, ApJ, 608, 16
- Zehavi, I., Zheng, Z., Weinberg, D. H., Frieman, J. A., Berlind, A. A., et al. 2004, ApJ (submitted), (astro-ph/0408569)
- Zheng, Z. 2004, ApJ, 610, 61
- Zheng, Z., Tinker, J. L., Weinberg, D. H., & Berlind, A. A. 2002, ApJ, 575, 617
- Zheng, Z., Berlind, A. A., Weinberg, D. H., Benson, A. J., Baugh, C. M., Cole, S., Davé, R., Frenk, C. S., Katz, A., & Lacey, C. G. 2004, ApJ (submitted) astro-ph/0408569

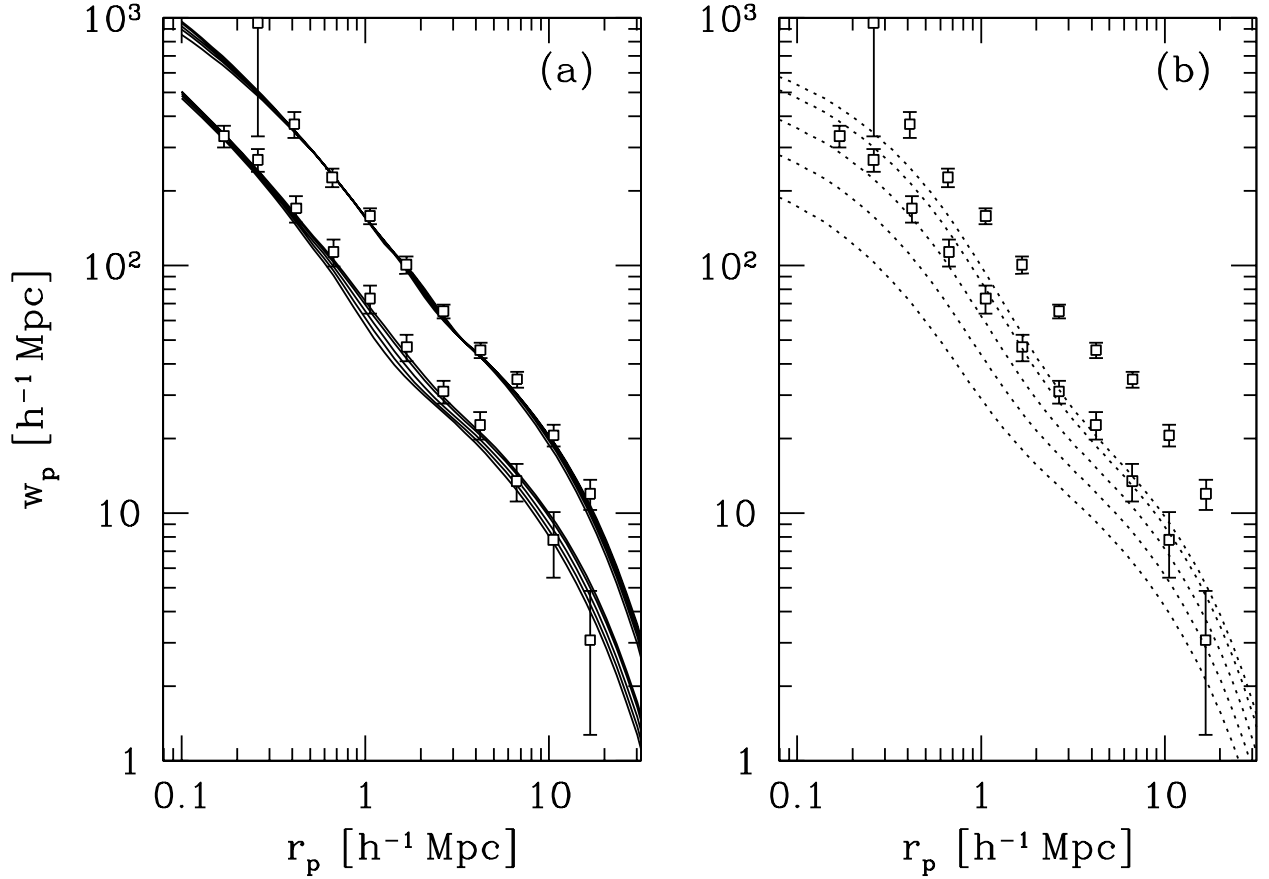


Fig. 1.— (a) The HOD fits are compared to the  $w_p(r_p)$  data for galaxy samples  $M_r < -20$  (lower points) and  $M_r < -21.5$  (upper points). The five solid curves represent the five values of  $\sigma_8$ , with the lowest curve being  $\sigma_8 = 0.6$  in both fits, and each subsequent curve going in order of increasing  $\sigma_8$ . (b) The projected dark matter correlation functions for  $\Omega_m = 0.3$  and all five values of  $\sigma_8$ . The curves, from lowest to highest, go in order of increasing  $\sigma_8$ . For comparison, the  $w_p(r_p)$  data are plotted as well.

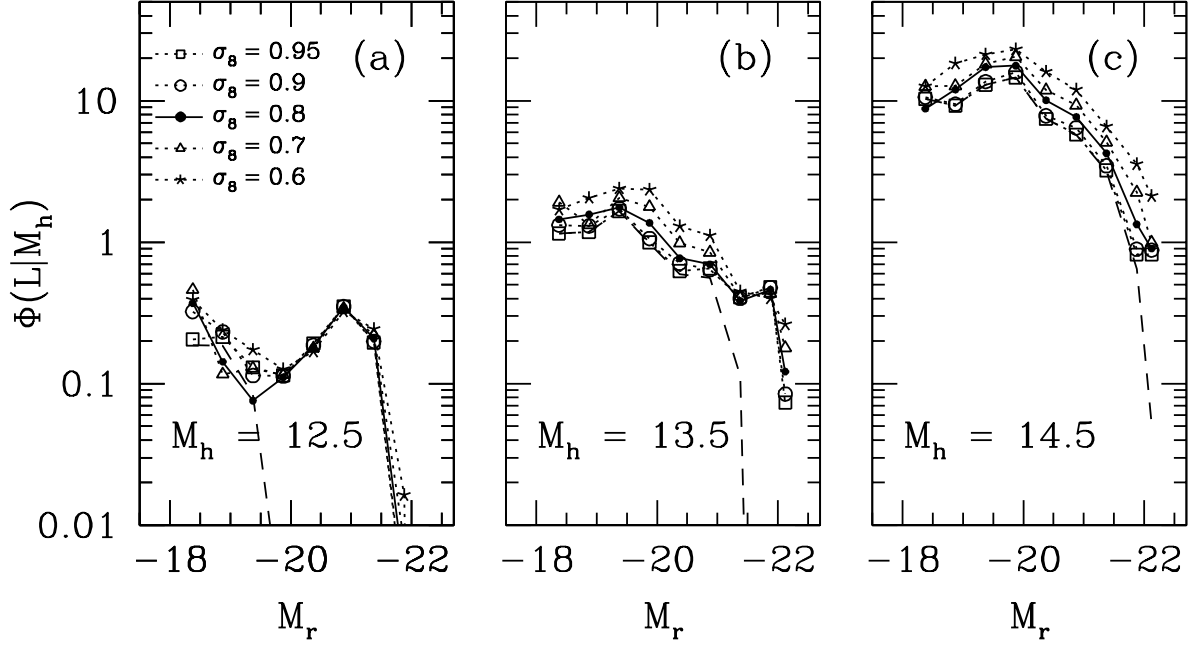


Fig. 2.— The conditional luminosity function,  $\Phi(L|M_h)$ , is plotted for three different halo masses,  $\log(M_h/M_\odot) = 12.5, 13.5,$  and  $14.5$ , and for all five values of  $\sigma_8$ . The curves are all normalized such that the area under each curve is  $\langle N \rangle_M$  for  $M_r < -18$ . The dashed line in each plot is an example of the contribution to  $\Phi(L|M_h)$  by satellite galaxies only (here for  $\sigma_8 = 0.95$ ). At  $M = 3 \times 10^{12} h^{-1} M_\odot$ , satellites contribute only to the faint end of  $\Phi(L|M_h)$ , while for the cluster-mass halos of panel (c), satellites dominate the luminosity function for all but the brightest magnitude bin.

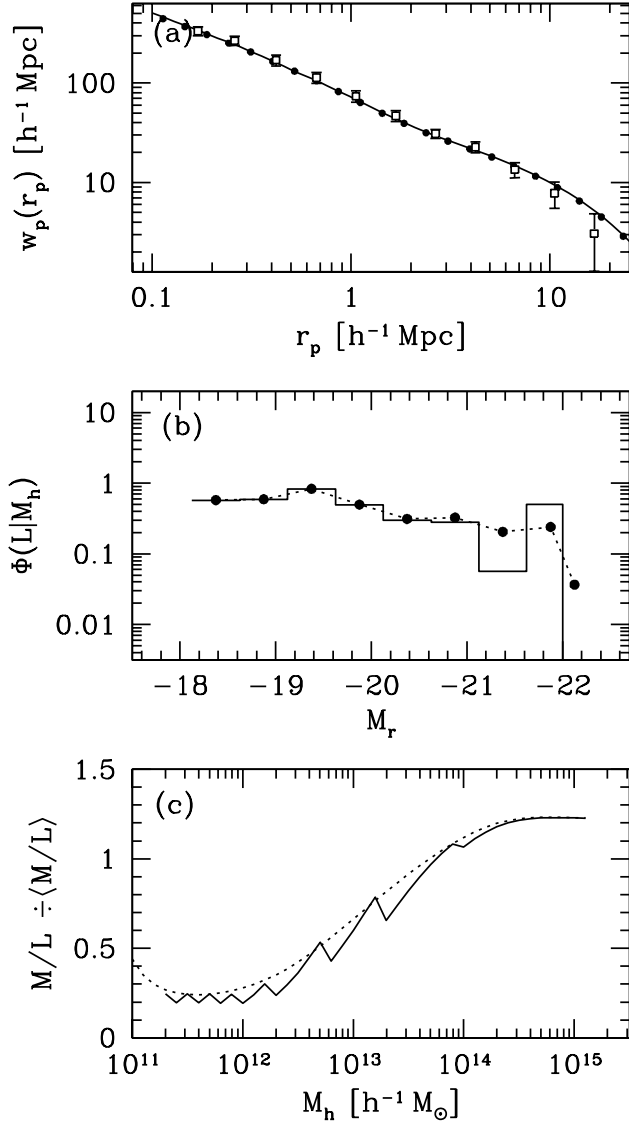


Fig. 3.— A comparison between soft and hard central galaxy cutoffs. Panel (a) demonstrates that the different central occupation functions do not change the predicted  $w_p(r_p)$ . The open squares are the data for  $M_r < -20$  galaxies from Zehavi et al. (2004b). The solid line is the HOD fit to the data using a hard cutoff. The solid circles represent the same HOD parameters, but  $w_p(r_p)$  is recalculated for a soft cutoff. Panel (b) shows the difference in  $\Phi(L|M_h)$  from the two methods for  $M = 3 \times 10^{13} h^{-1} M_\odot$ . A hard cutoff, shown with the solid histogram, produces a significant bump at  $M_r \sim -22$ , which is smoothed out by the soft cutoff, shown by the dotted line and filled circles. Panel (c) shows the  $M/L$  ratio as a function of halo mass for the two methods. The solid line represents the hard cutoff and the dotted lines represents the soft cutoff. The differences are small, and nearly negligible at high masses.

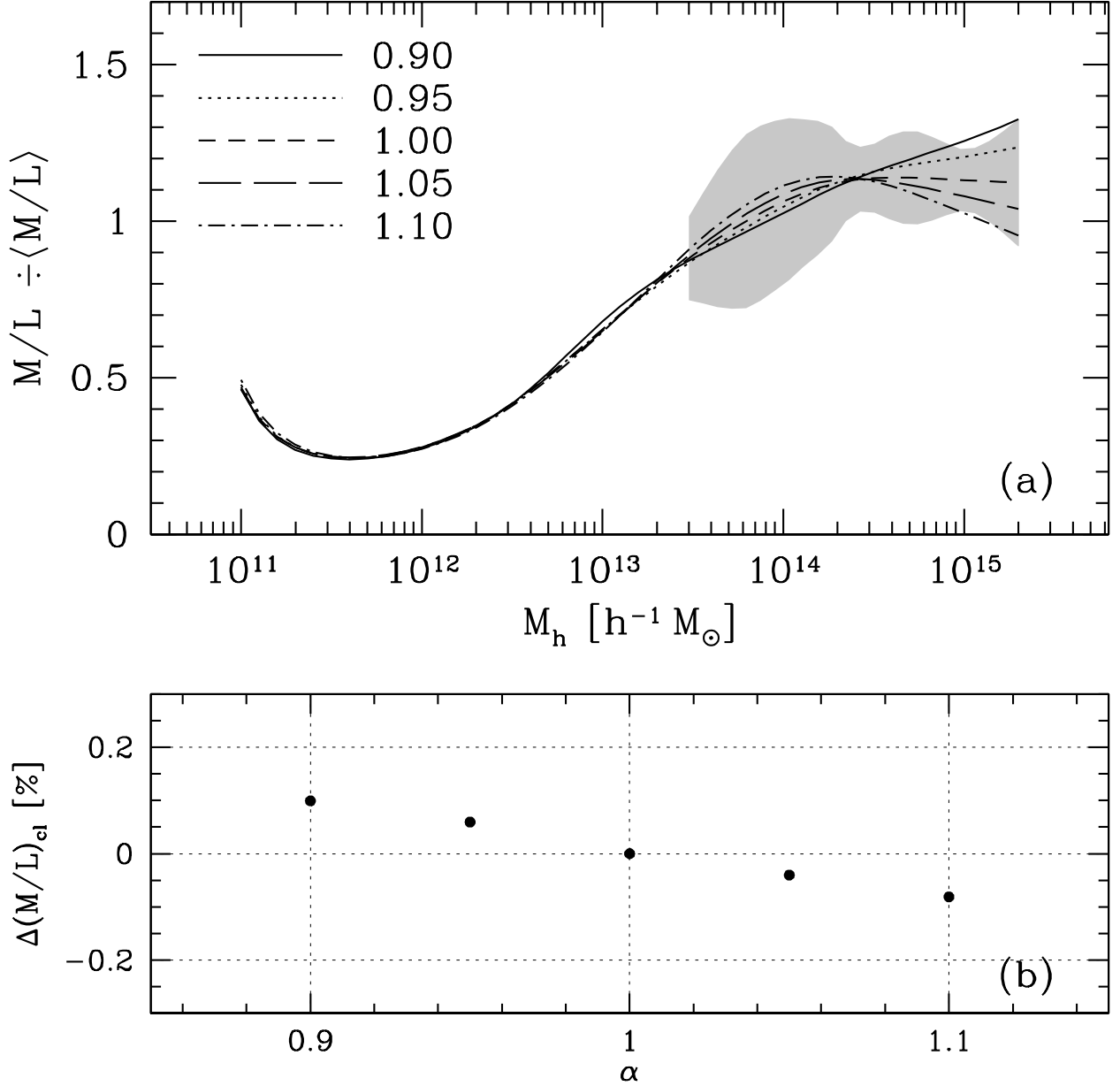


Fig. 4.— (a)  $M/L$  ratio as a function of halo mass for five values of  $\alpha$ : 0.9, 0.95, 1.0, 1.05 and 1.1. All calculations assume  $\sigma_8 = 0.9$ . The shaded region is the full-width at 10% maximum of the distribution of halo  $M/L$  inferred from a flexible HOD parameterization with no fixed value of  $\alpha$ . See text for further details. (b) The change in the mean cluster  $M/L$  ratio as a function of  $\alpha$  relative to  $\alpha = 1$ . The mean is calculated for the same distribution of cluster masses as the CNOC cluster sample.

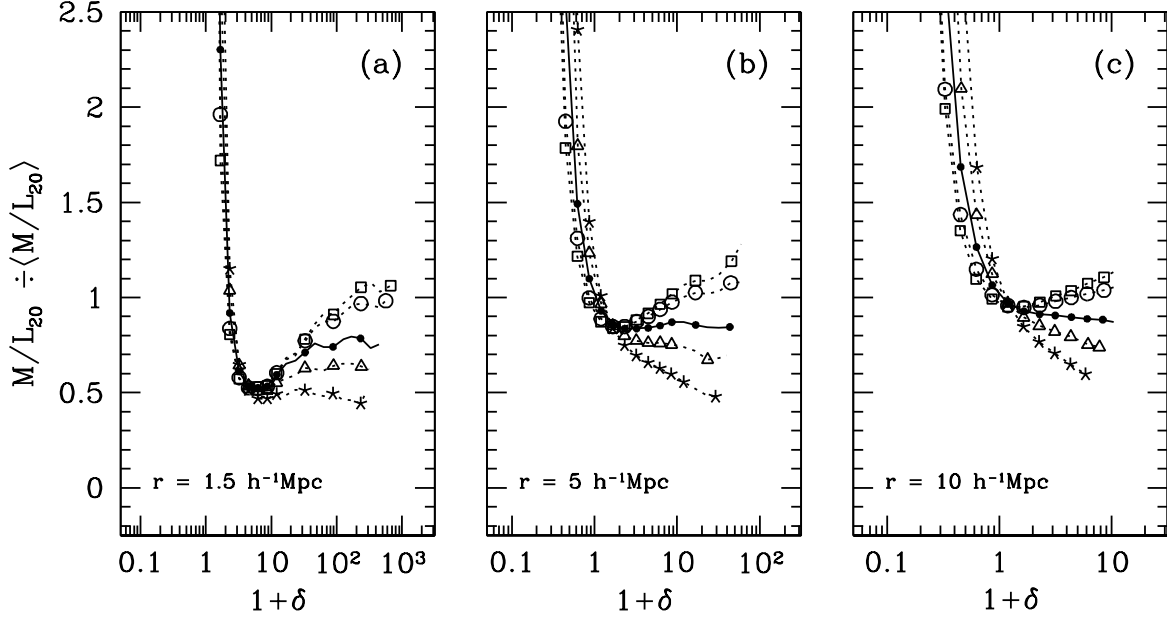


Fig. 5.— The mean  $M/L$  ratio in spheres of radius  $r$  as a function of the enclosed overdensity  $1 + \delta$ , for  $r = 1.5, 5.0,$  and  $10.0 \text{ h}^{-1} \text{ Mpc}$  (panels a, b, and c, respectively). Results are calculated from the numerical simulations and refer to luminosities of galaxies with  $M_r < -20$ . Different symbols represent different  $\sigma_8$  values with the same coding as Figure 2; at high  $\delta$ , the  $\sigma_8 = 0.6$  curve is always lowest.

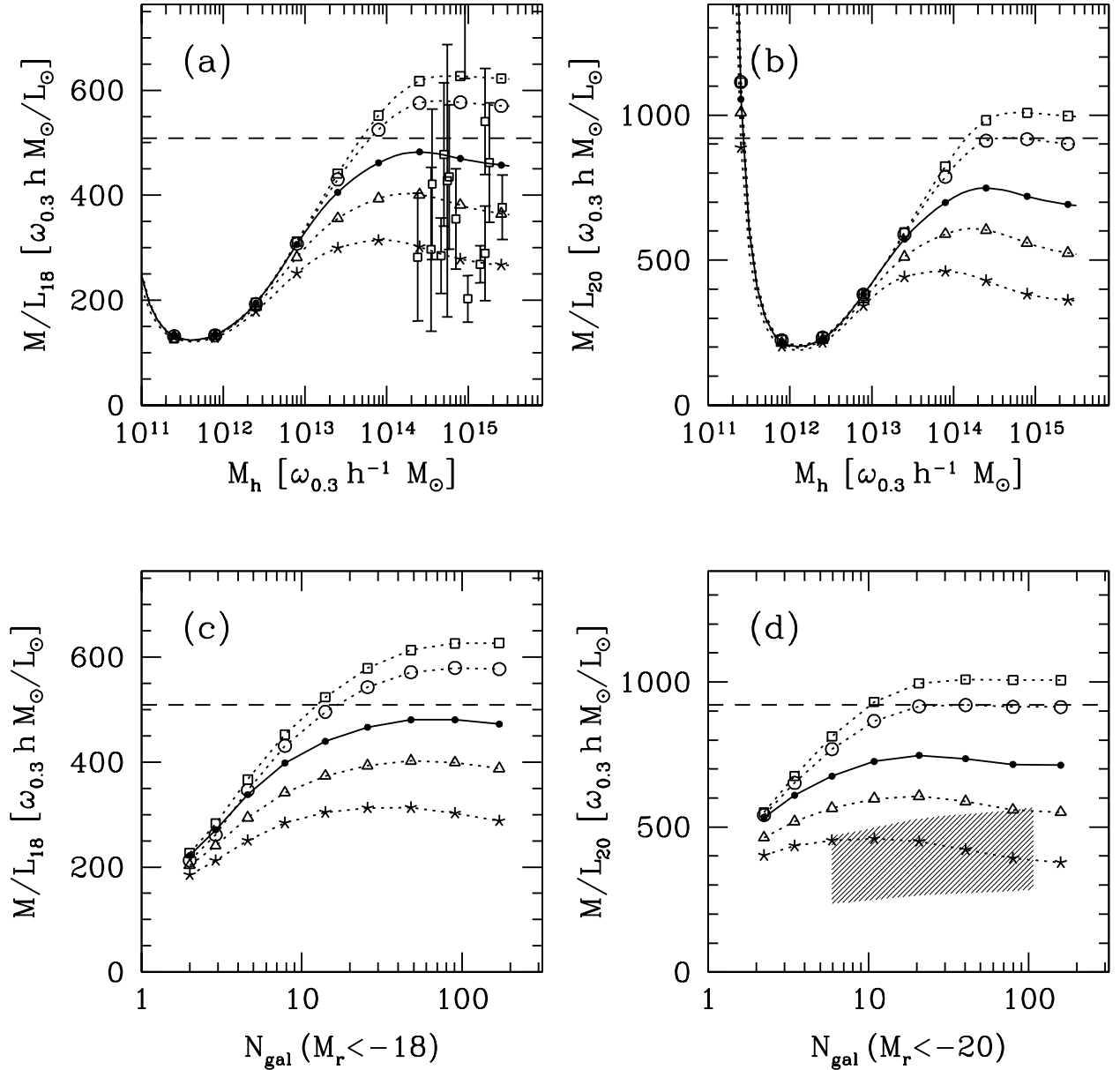


Fig. 6.— Mass-to-light ratio ( $r$ -band) as a function of halo mass (top panels) or richness (bottom panels). Luminosities are for galaxies brighter than  $M_r = -18$  (left) and  $M_r = -20$  (right). From bottom to top, curves represent  $\sigma_8 = 0.6, 0.7, 0.8, 0.9, 0.95$ . Dashed horizontal lines represent the mean  $M/L$  of the universe. In panel (a), open squares with error bars are the CNOc data of Carlberg et al. (1996). In panel (d), the shaded region represents the  $M/L$  ratio of SDSS clusters based on Bahcall et al. (2003a).

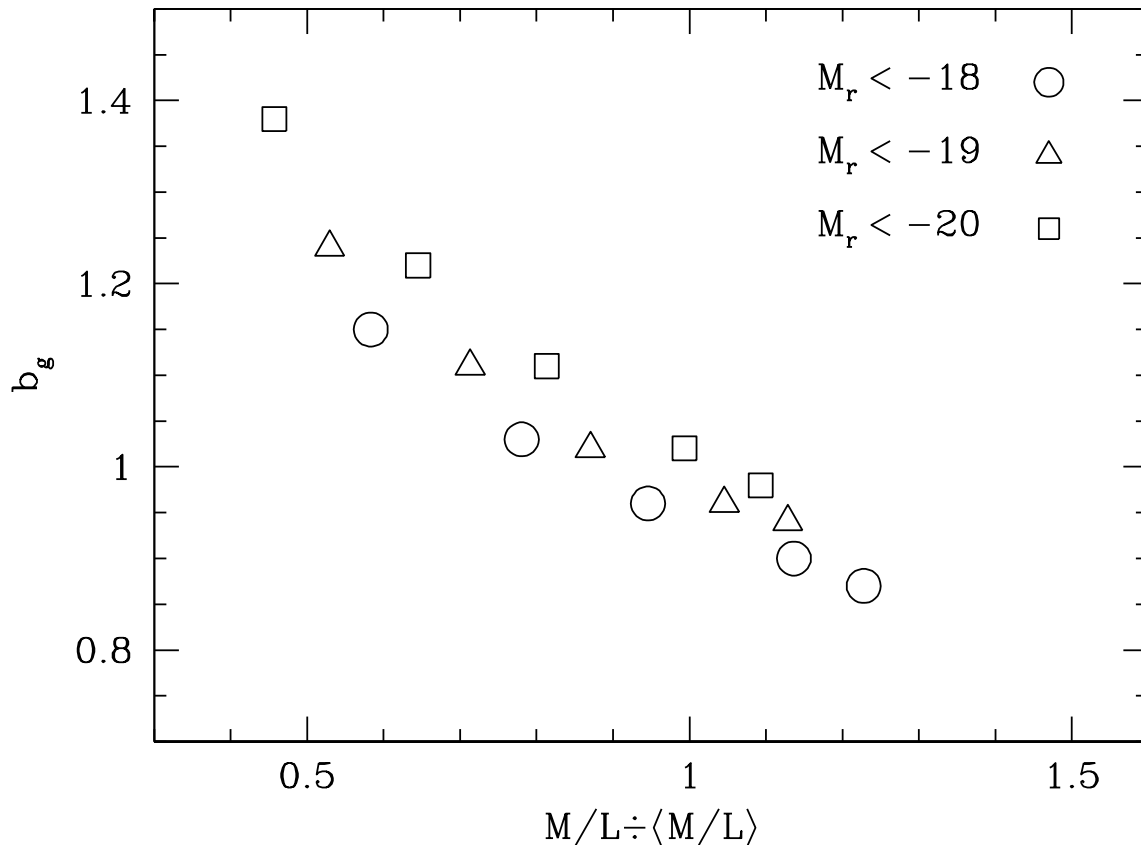


Fig. 7.— Galaxy bias, calculated for the SDSS samples from our HOD models, as a function of mass-to-light ratio at  $M = 5 \times 10^{14} \omega_{0.3} h^{-1} M_{\odot}$ , relative to  $\langle M/L \rangle$ . The different plot symbols represent three different galaxy magnitude thresholds,  $M_r = -18, -19$ , and  $-20$ . For each sample, the data points represent the five different  $\sigma_8$  values used. The data always follow the monotonic trend of increasing  $\sigma_8$  for decreasing  $b_g$  (e.g.,  $\sigma_8 = 0.6$  at the far left and  $\sigma_8 = 0.95$  at the far right).

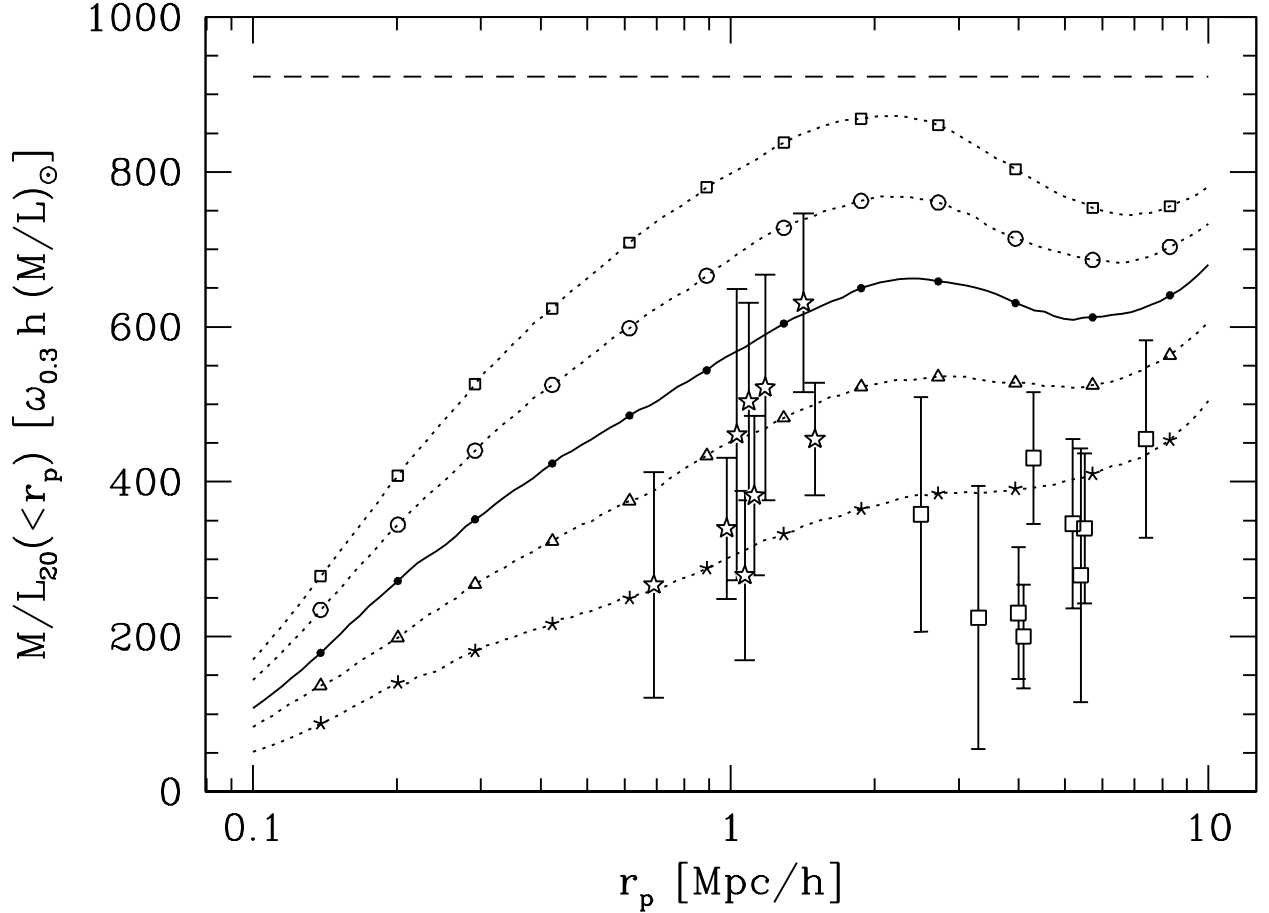


Fig. 8.— Mean  $M/L$  ratios of clusters (with  $M > 3 \times 10^{14} h^{-1} M_{\odot}$ ) as a function of projected separation from the cluster center, calculated from the numerical simulations. from bottom to top, the curves represent  $\sigma_8 = 0.6, 0.7, 0.8, 0.9, 0.95$ . Following Rines et al. (2004), we calculate masses in spheres and luminosities (for  $M_r \geq -20$ ) in truncated cylinders, which depresses  $M/L$  values below those shown in Figures 6b and 6d. Stars and open squares represent the  $M/L$  estimates of Rines et al. (2004) at  $r_{200}$  and cluster turnaround radii, respectively, converted from  $K$ -band to  $r$ -band as described in the text. The dashed horizontal line shows the mean  $M/L_{20}$  of the box.

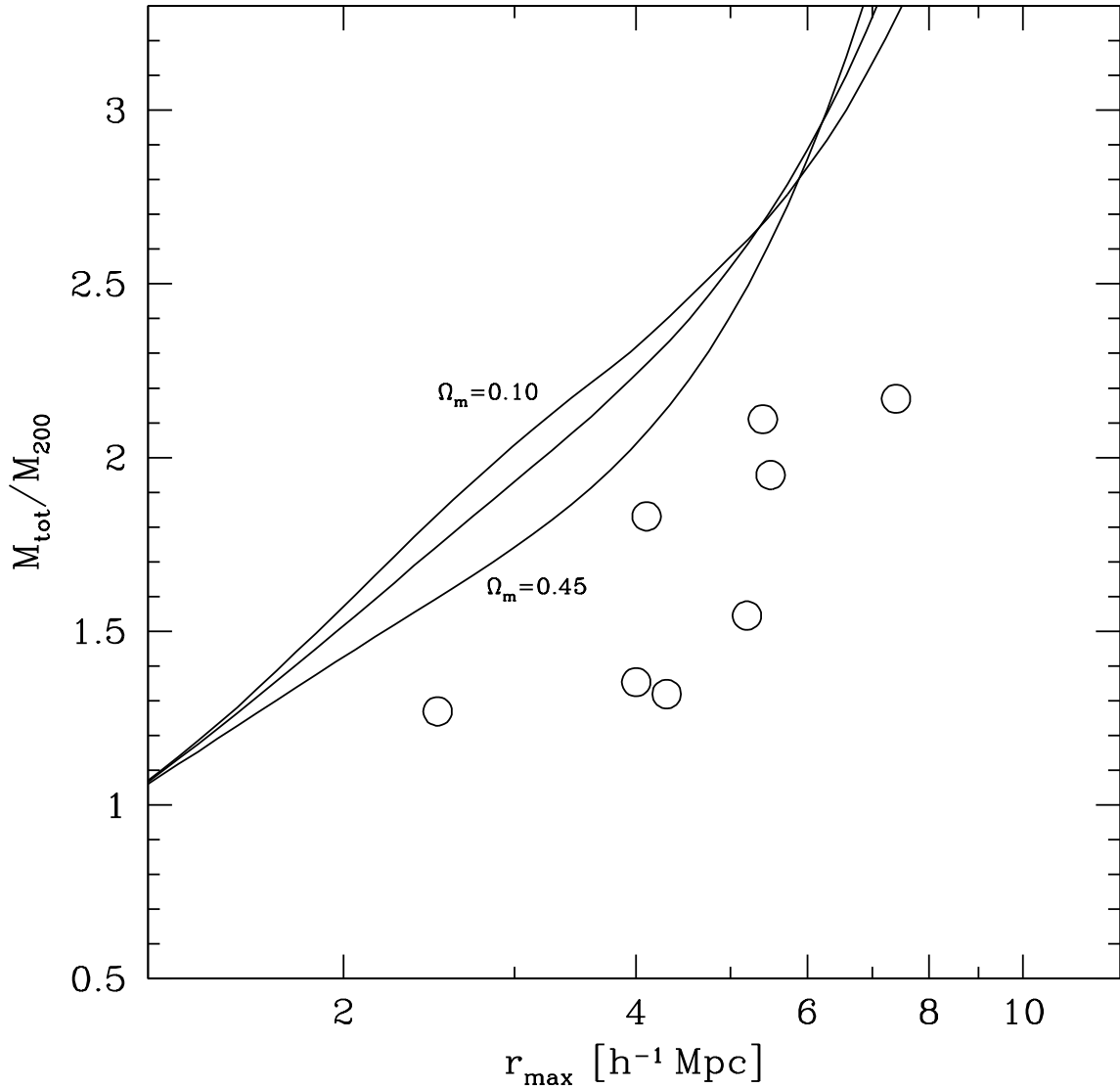


Fig. 9.— Ratio of the total mass within  $r_{\text{max}}$  to the mass within  $r_{200}$  from the Rines et al. (2004) data (open circles) and our simulations (curves). The predictions depend slightly on the value of  $\Omega_m$  assumed in calculating cluster masses, since we consider only halos with  $M \geq 3 \times 10^{14} h^{-1} M_{\odot}$ . The curves represent  $\Omega_m = 0.1, 0.3$ , and  $0.45$ , and are calculated for  $\sigma_8 = 0.8$ ; results for other  $\sigma_8$  are similar.

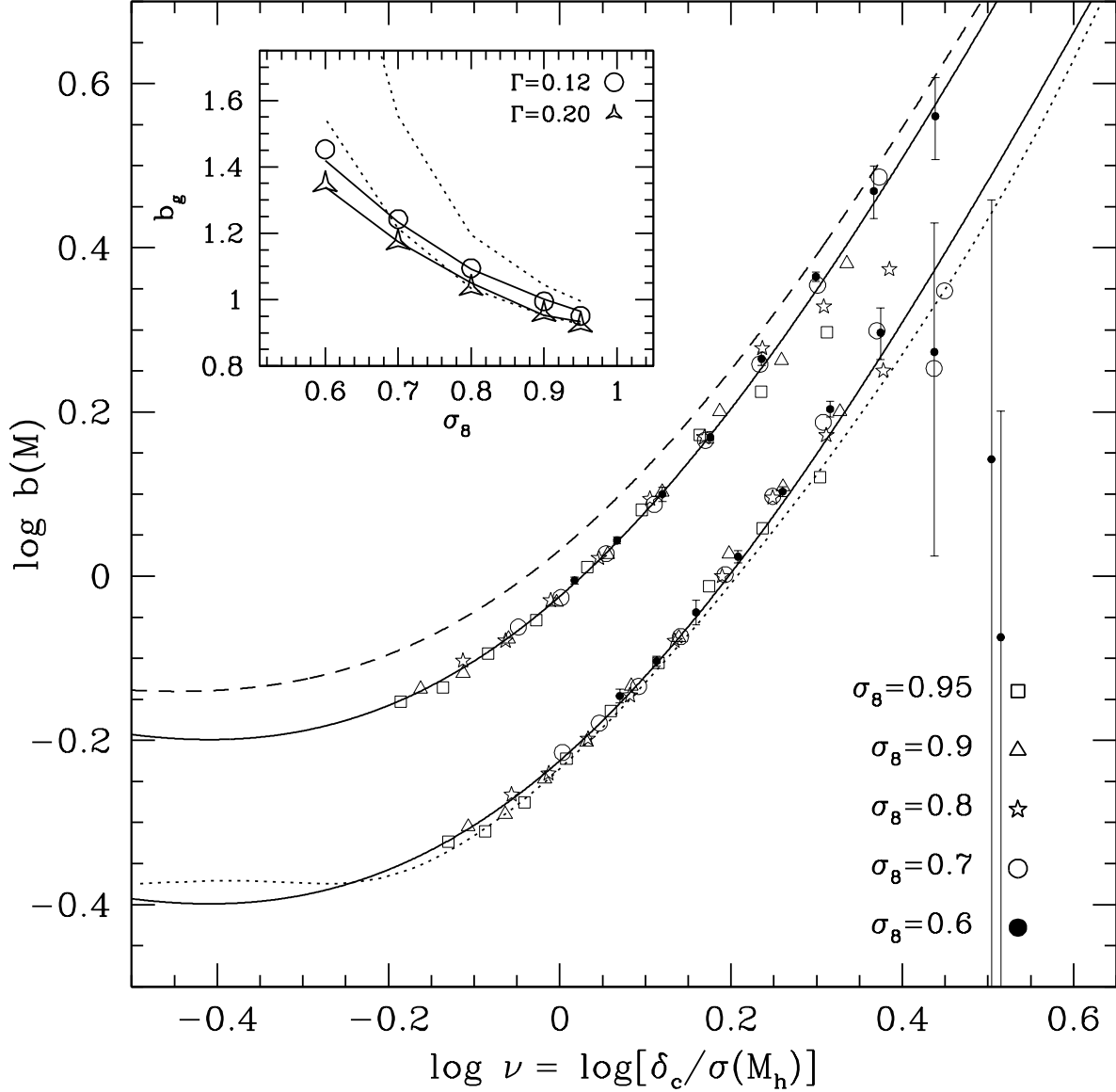


Fig. 10.— The halo bias factor is shown as a function of  $\nu$  for the five different values of  $\sigma_8$  for both  $\Gamma = 0.2$  and  $\Gamma = 0.12$ . The values of the bias factor were calculated from the asymptotic value of the correlation function at large scales:  $b_h = \sqrt{\xi_h/\xi_m}$ . The  $\Gamma = 0.12$  results are offset by 0.2 dex to avoid crowding. The dashed line is the bias relation given by Sheth, Mo, & Tormen (2001). The solid line shows the bias relation of the same functional form, but using the parameters  $a = 0.707$ ,  $b = 0.35$ , and  $c = 0.80$ . The dotted line is the bias relation of Seljak & Warren (2004) calculated for  $\sigma_8 = 0.9$  and  $\Gamma = 0.2$ . The error bars, shown only for  $\sigma_8 = 0.6$ , are the error in the mean of the five realizations. *Inset box*: The galaxy bias parameter for the HOD models of Tinker et al. (2005), plotted as a function of  $\sigma_8$ . The solid lines are analytic calculations of the galaxy bias using the new bias relation. The dotted lines are the analytic calculations of  $b_g$  using the bias relation of Seljak & Warren (2004).

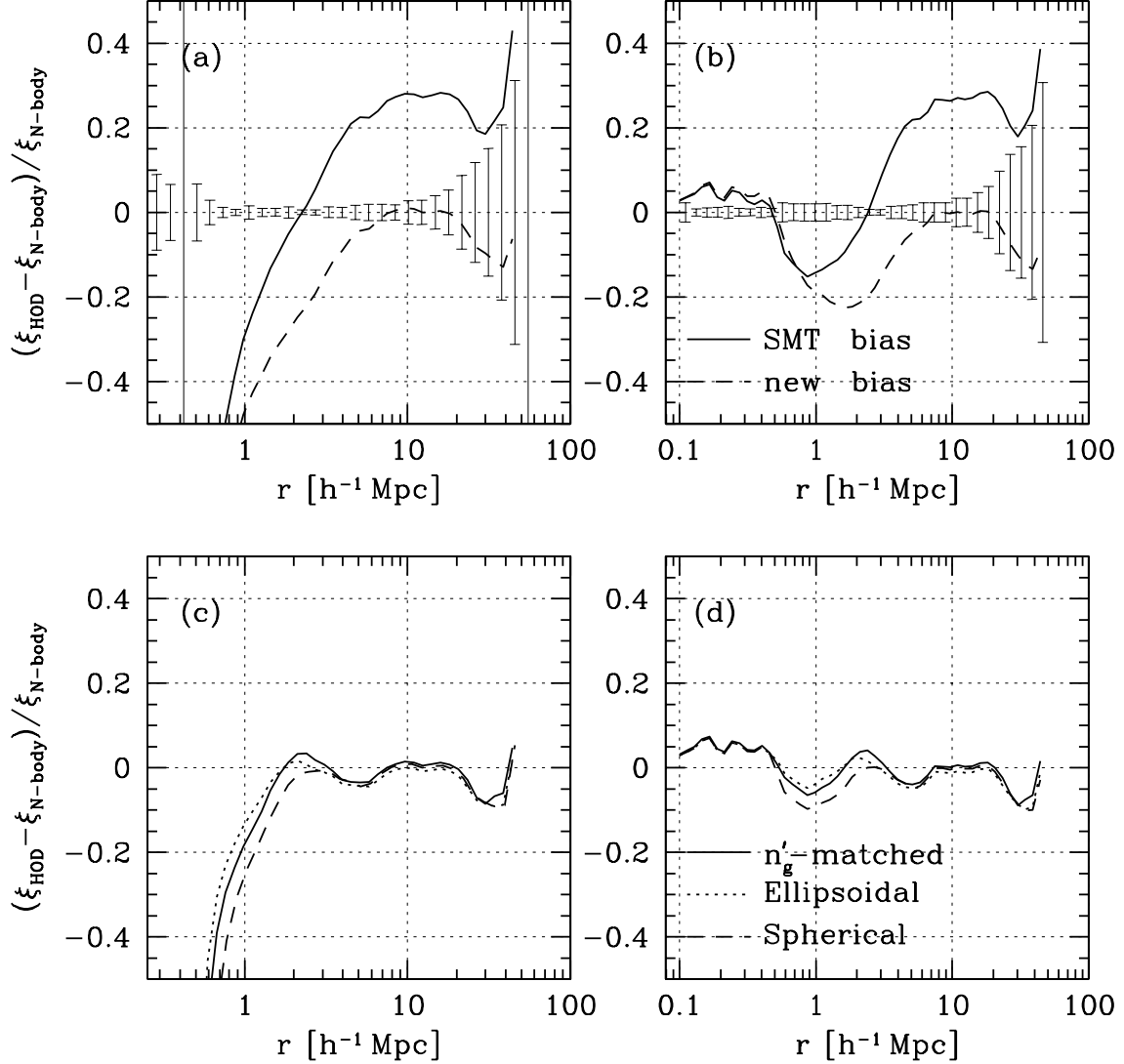


Fig. 11.— The analytic HOD calculation of  $\xi_g(r)$  is compared to numerical results for different bias and halo exclusion prescriptions. Panel (a): The calculation of  $\xi_{2h}$  using the halo exclusion approach of Zheng (2004) is compared to N-body results. The solid line the calculation performed with the halo bias prescription of Sheth, Mo, & Tormen (2001). The dashed line is the same calculation using the modified bias in Appendix A. The error bars represent the error in the mean from the five realizations. Panel (b) compares the total calculation of  $\xi_g(r)$  with the numerical results. Panels (c) and (d) compare  $\xi_{2h}$  and  $\xi_g(r)$  calculated by the three new halo exclusion methods described in Appendix B to the N-body results.